Han *et al.*
Chinese Journal of Mechanical Engineering (2023) 36:77
https://doi.org/10.1186/s10033-023-00899-1

Chinese Journal of Mechanical Engineering

ORIGINAL ARTICLE

Open Access

Task-Oriented Topology System Synthesis of Reconfigurable Legged Mobile Lander Integrating Active and Passive Metamorphoses

Youcheng Han[1], Ziyue Li[1], Gaohan Zhu[1], Weizhong Guo[1*], Jianzhong Yang[2] and Wei Liu[2]

Abstract

To explore hostile extraterrestrial landforms and construct an engineering prototype, this paper presents the task-oriented topology system synthesis of reconfigurable legged mobile lander (ReLML) with three operation modes from adjusting, landing, to roving. Compared with our preceding works, the adjusting mode with three rotations (3R) provides a totally novel exploration approach to geometrically matching and securely arriving at complex terrains dangerous to visit currently; the landing mode is redefined by two rotations one translation (2R1T), identical with the tried-and-tested Apollo and Chang'E landers to enhance survivability via reasonable touchdown buffering motion; roving mode also utilizes 2R1T motion for good motion and force properties. The reconfigurable mechanism theory is first brought into synthesizing legged mobile lander integrating active and passive metamorphoses, composed of two types of metamorphic joints and metamorphic execution and transmission mechanisms. To reveal metamorphic principles with multiple finite motions, the finite screw theory is developed to present the procedure from unified mathematical representation, modes and source phase derivations, metamorphic joint and limb design, to final structure assembly. To identify the prototype topology, the 3D optimal selection matrix method is proposed considering three operation modes, five evaluation criteria, and two topological subsystems. Finally, simulation verifies the whole task implementation process to ensure the reasonability of design.

Keywords Legged mobile lander, Topology synthesis, Active and passive metamorphoses, Finite screw, Metamorphic joint, Reconfigurable mechanism

1 Introduction

1.1 On Legged Designs for In-Situ Extraterrestrial Exploration

Legged designs for in-situ extraterrestrial exploration have the merits of lightweight, good stability, large payload, good locomotion, operation capabilities, etc [1, 2]. Typical ones are revisited: (1) The tripod-type legged lander with passive buffering has achieved success in the landers like Surveyor [3], Luna [4], Tianwen [5], Phoenix [6], etc. It usually has $RP_bR\&2R$ and $RR\&2UP_bS$ topologies with 1−2 buffering DOFs (R, U, S-revolute, universal, spherical joints, P_b-buffering damper), etc. The advantages of lightweight and high folding ratio make it widely used for the tentative in-situ exploration; (2) the cantilever-type legged lander with passive buffering contributes to the landers like Apollo [7], Chang'E [8], etc. It usually has the $(2UP_bS\&U)$-P_b topology and three buffering DOFs, with merits of large payload and high stability to carry rover, human, cargo, and instrument for mobile detection; (3) the hybrid wheel-legged rover, such as the six-legged Athlete with 6-DOF serial leg for cargo handling and manipulation [9], the four-legged Mars rover SherpaTT with 5-DOF planar leg [10], etc.; (4) the legged

*Correspondence:
Weizhong Guo
wzguo@sjtu.edu.cn
[1] State Key Lab of Mechanical System and Vibration, School of Mechanical Engineering, Shanghai Jiao Tong University, Shanghai 200240, China
[2] Beijing Institute of Spacecraft System Engineering, Beijing 100094, China

robot with active landing. Yin et al. [11, 12] presented a six-legged mobile lander with 3-DOF hybrid leg for active landing and walking control on the planet; Kolvenbach et al. [13] designed a four-legged robot with 2-DOF parallel leg for the cat-like jumping and landing on the asteroid, etc.

However, the tripod-type legged lander is immovable for the fixed-point detection; the cantilever-type legged lander launches both legged stationary lander and rover for mobile detection around landing point, but it wastes a large transport resource and produces some technical shortages on redundant machinery, electronics, control, sensing, communication, power, support, etc.; the hybrid wheel-legged rover in essence doesn't have buffering ability, so it must be carried by a lander; the legged robot with active landing also integrates the locomotion ability, but the active landing brings much pressure to motor and wastes much energy supply. This determines it cannot carry heavy cargo or human for landing on the high-gravitational planet. Consequently, our group has put forward the novel legged mobile lander, including the studies on basic concept [14, 15], decoupled landing and walking functions [16–18], singularity and passive limb based synthesis [19, 20], etc.

Nevertheless, challenges still exist when designing the practical engineering prototype of ReLML. (1) On operation mode. Preceding studies focus on landing and roving modes, haven't considered adjusting mode—match touchdown pose of leg truss for complex terrains and enhance landing adaptability. This work aims at three-mode synthesis from adjusting, landing, to roving. Moreover, preceding studies see landing leg as a 0-DOF truss, but synthesize it with 1R characteristic due to fold and deployment, and neglect the buffering damper arrangements and mobility effects. Differently, this study redefines landing mode with 3 buffering DOFs and 2R1T buffering motions by truss-mechanism transformation [17]. (2) On topology synthesis fundamental. Preceding studies use the manifold synthesis method [21] twice to obtain landing and roving topologies. No convictive reason is given on how to combine them into a unified one, so the mode switch and reconfiguration are not strongly deduced. This work takes metamorphic theory for the three-mode synthesis of ReLML, and presents a rigorous procedure from unified mathematical representation, modes and source phase derivations, metamorphic joint and limb design, to structure assembly. Finite screw theory [22–25] is used to demonstrate metamorphic principles with multiple finite motions. (3) Topological thinking on feasibility and reliability. The reconfigurable joint should be carefully argued due to its effects on theoretical reconfigurability (topology, motion type, range, switch, etc.) and practical reliability (payload, impact resistance, technical simplicity, controllability, etc.). Also, the numbers of closed-loops, limbs, joints should be as few as possible to improve payload and stiffness. The actuation-transmission system should be separated from execution, to avoid the touchdown impact flow going through fragile actuation parts like motor, sensor, encoder, reducer, etc.

1.2 On Topology Design of Reconfigurable Mechanism

The topology synthesis of reconfigurable mechanism has gradually formed into an axiomatic system based on adjacency matrix [26], unified topological graph [27], augmented Assur group [28], etc. Furthermore, Kong et al. [29] established the screw-based synthesis approach for the multi-mode mechanism; Jin et al. [30] presented the synthesis method by the variable constraint screw system; Li and Hervé [31] introduced the manifold synthesis method into the parallel mechanism with bifurcated motion; Wei and Dai [32, 33] showed a systematic synthesis method of both metamorphic and multi-mode mechanisms using group and manifold operation; Yao et al. [34–36] presented in-depth works on legged robot reconfigured by metamorphic joint and constraint singularity control. The graphical method by Yu et al. [37, 38] provided significant references to novel buffering principle and design integrating tuned mass damper. To identify the optimal topology, Shen et al. [39] proposed systematic topological evaluation indices, so mechanisms with motion decoupling, symbolic forward solution, fewer input–more output properties are invented [40, 41]; He et al. [42] measured the type complexity upon kinematic pair and geometric constraint; Hüsing et al. [43] reported a quantitative assessment method scored by nine criteria, etc.

Although the above make certain achievements, challenges also exist for the aerospace-task-demanded topology design of ReLML: (1) Current theoretical system hasn't well considered influences of multiple working conditions on complex extraterrestrial environments; (2) landing mode has a large impact response and roving mode requires a high loading capability. Mechanism and joint must meet reconfigurability and engineering value; (3) current metamorphic mechanisms mostly take active metamorphosis by specialized devices to switch joint's motion axis. There seems few passive metamorphosis—change topology and mobility by the external force. This study aims to integrate both active and passive metamorphoses into ReLML: Landing mode is passively reconfigured by footpad-soil touchdown impact, adjusting and roving modes are actively reconfigured by motors.

2 Procedures for the Task-Oriented Topology System Synthesis of ReLML

Soft-landing detection probes have yet been restricted to arrive at flat and friendly areas on extraterrestrial bodies. They still cannot reach hostile terrains, such as mountain, canyon, gully, slope, rock, pit, etc. These environments are more likely to conserve the original planet evolution information, and help to analyze geological changes and resource distribution. Given such a bottleneck, a tailored task-oriented design method is proposed for the novel probe as follows.

Step 1: Define the reconfigurable legged mobile lander (ReLML), capable of in-situ exploration for complex extraterrestrial environments. Three operation modes are endowed: adjusting mode geometrically matches the leg truss's touchdown pose for various terrains, to enhance the environment adaptability and securely arrive at broader areas; landing mode adopts buffering dampers to absorb touchdown impact energy, during which the damper-constructed truss behaves mechanism kinematic and dynamic properties with large displacement and mobility [19]; roving mode implements legged mobile detection. At the start of design, the topology system graph is defined by the designer's subjective initiative. Active and passive metamorphoses lie in the metamorphic joint, execution, and transmission of ReLML.

Step 2: Identify output finite motions in each mode. Demonstrate number synthesis for common finite motions, and determine numbers of DOFs, metamorphic joints, metamorphic limbs, buffering dampers, actuations, etc.

Step 3: Represent the finite motions of metamorphic joints, single leg, and overall lander in three operation modes. The finite screw is employed.

Step 4: Synthesize the metamorphic execution mechanism with three modes of adjusting, landing, and roving. Firstly, determine the kinematic bond of the metamorphic limb; then, design the mechanical generator for the metamorphic joint and limb followed by assembling them. Via the topology evolution, the metamorphic hybrid topologies are obtained from the parallel ones. Thus, both cantilever- and tripod-type landing trusses are embedded in this study, whose successes can enhance engineering practicability.

Step 5: Synthesize the metamorphic transmission mechanism. Initially, propose the equivalent metamorphic parallel mechanism model to describe the topological correlations between execution limb and transmission. Then, identify the multi-mode output motion and number synthesis; next, determine kinematic bond of transmission limb followed by structural design and assembly.

Step 6: Multi-mode & multi-criterion optimal selection and simulation. Executions and transmissions are measured respectively in multi-modes by five criteria. After identifying the optimal combination, simulation is used to verify reconfigurability and operation behaviors.

Topology system mapping graph of the prototype is shown in Figure 1. Metamorphic execution plays a direct participant role in three modes to interact with the environment. The metamorphic active joint has two switchable motion axes between adjusting and roving and a reliable rigid phase in landing mode. The metamorphic passive joint (buffering damper) is made of plastic aluminum honeycomb. Metamorphic transmission is arranged to protect the fragile actuation against large impact, also makes single-input multi-output differences to power the operation and mode switch. In the graph, ${}^{ex}E_k$ is the kth execution end-effector. P_{bj}, ${}^{ex}L_j$, J_{mj}, ${}^{tr}E_j$ are the jth buffering damper, execution limb, metamorphic active joint, transmission end-effector respectively in the kth leg, n_{ex} is the number of execution limb. ${}^{tr}L_h^j$, ${}^{tr}A_h^j$ are the hth transmission limb and actuation respectively for the jth execution limb, n_{tr} is the number of transmission limb.

3 Determine Multi-Mode Finite Motion Submanifolds and Number Synthesis

To exclude the local mobility of the spherical joint for footpad-terrain adaptation, the ankle link is taken as moving platform. In this study, the output finite motion submanifold of adjusting mode is assigned with 3R for large orientation adjustment to match undulating terrains. Those of landing and roving modes are assigned with double 2R1T for good motion and force properties to survive in complex environments. Their representations by finite screw format are given as

$$\left\{{}^{\mathrm{m}}\boldsymbol{S}_{f,Leg,3\mathrm{R}}\right\}_{\mathrm{m}=a} = \left\{2\tan\frac{\theta_{a3}}{2}\begin{pmatrix}\boldsymbol{s}_{a3}\\ \boldsymbol{r}_{a3}\times\boldsymbol{s}_{a3}\end{pmatrix}\Delta 2\tan\frac{\theta_{a2}}{2}\begin{pmatrix}\boldsymbol{s}_{a2}\\ \boldsymbol{r}_{a2}\times\boldsymbol{s}_{a2}\end{pmatrix}\Delta 2\tan\frac{\theta_{a1}}{2}\begin{pmatrix}\boldsymbol{s}_{a1}\\ \boldsymbol{r}_{a1}\times\boldsymbol{s}_{a1}\end{pmatrix}\right\}, \tag{1}$$

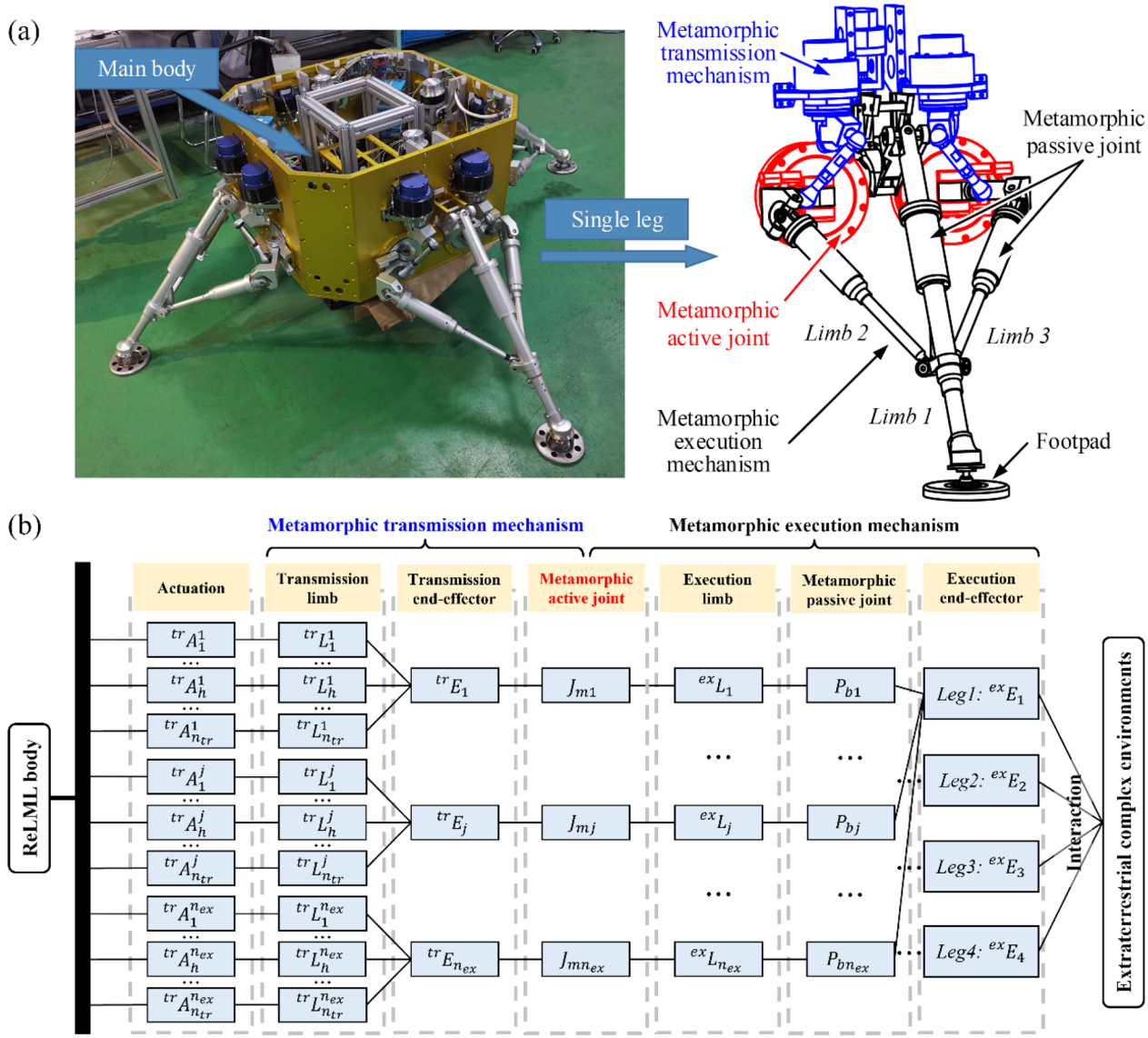

Figure 1 ReLML integrating active and passive metamorphoses: **a** Prototype construction, **b** Topology system mapping graph

$$\left\{{}^{\mathrm{m}}\boldsymbol{S}_{f,Leg,2\mathrm{R1T}}\right\}_{\mathrm{m}=l,r}=\begin{cases}\left\{2\tan\dfrac{\theta_{\mathrm{m3}}}{2}\begin{pmatrix}\boldsymbol{s}_{\mathrm{m3}}\\ \boldsymbol{r}_{\mathrm{m3}}\times\boldsymbol{s}_{\mathrm{m3}}\end{pmatrix}\Delta 2\tan\dfrac{\theta_{\mathrm{m2}}}{2}\begin{pmatrix}\boldsymbol{s}_{\mathrm{m2}}\\ \boldsymbol{r}_{\mathrm{m2}}\times\boldsymbol{s}_{\mathrm{m2}}\end{pmatrix}\Delta t_{\mathrm{m1}}\begin{pmatrix}\boldsymbol{0}\\ \boldsymbol{s}_{\mathrm{m1}}\end{pmatrix}\right\},\\ \left\{2\tan\dfrac{\theta_{\mathrm{m3}}}{2}\begin{pmatrix}\boldsymbol{s}_{\mathrm{m3}}\\ \boldsymbol{r}_{\mathrm{m3}}\times\boldsymbol{s}_{\mathrm{m3}}\end{pmatrix}\Delta t_{\mathrm{m2}}\begin{pmatrix}\boldsymbol{0}\\ \boldsymbol{s}_{\mathrm{m2}}\end{pmatrix}\Delta 2\tan\dfrac{\theta_{\mathrm{m1}}}{2}\begin{pmatrix}\boldsymbol{s}_{\mathrm{m1}}\\ \boldsymbol{r}_{\mathrm{m1}}\times\boldsymbol{s}_{\mathrm{m1}}\end{pmatrix}\right\},\\ \left\{t_{\mathrm{m3}}\begin{pmatrix}\boldsymbol{0}\\ \boldsymbol{s}_{\mathrm{m3}}\end{pmatrix}\Delta 2\tan\dfrac{\theta_{\mathrm{m2}}}{2}\begin{pmatrix}\boldsymbol{s}_{\mathrm{m2}}\\ \boldsymbol{r}_{\mathrm{m2}}\times\boldsymbol{s}_{\mathrm{m2}}\end{pmatrix}\Delta 2\tan\dfrac{\theta_{\mathrm{m1}}}{2}\begin{pmatrix}\boldsymbol{s}_{\mathrm{m1}}\\ \boldsymbol{r}_{\mathrm{m1}}\times\boldsymbol{s}_{\mathrm{m1}}\end{pmatrix}\right\},\end{cases}\tag{2}$$

where "m" denotes the source phase, adjusting, landing, roving modes respectively when $\mathrm{m}=o,\ a,\ l,\ r$. Herein, $\{\boldsymbol{S}_f\}$ is the submanifold (set) form of the finite screw $\boldsymbol{S}_f$ (element).

The finite motion of source phase is operated by union units of those of three modes, deduced as:

$$\left\{{}^{o}\boldsymbol{S}_{f,Leg}\right\} = \bigcup_{\mathrm{m}=a,l,r} \left\{{}^{\mathrm{m}}\boldsymbol{S}_{f,Leg}\right\}. \tag{3}$$

According to the intersection operation, there are at most two common finite motions between 3R and 2R1T, and three common ones between double 2R1T. Thus, Eq. (4) derives the dimension relationship of common finite motions between any two modes and among three modes.

$$\begin{aligned} &\dim\left(\bigcap_{\mathrm{m}=a,l}\left\{{}^{\mathrm{m}}\boldsymbol{S}_{f,Leg}\right\}\right) = \dim\left(\bigcap_{\mathrm{m}=a,r}\left\{{}^{\mathrm{m}}\boldsymbol{S}_{f,Leg}\right\}\right) \le 2, \\ &\dim\left(\bigcap_{\mathrm{m}=l,r}\left\{{}^{\mathrm{m}}\boldsymbol{S}_{f,Leg}\right\}\right) \le 3,\ \dim\left(\bigcap_{\mathrm{m}=a,l,r}\left\{{}^{\mathrm{m}}\boldsymbol{S}_{f,Leg}\right\}\right) \le 2. \end{aligned} \tag{4}$$

Employing the De Morgan's law to Eq. (3), the number synthesis principle can be derived by revealing dimension (or DOF) correlations of output motions of source phase, each mode, and the intersection of two/three modes.

$$\begin{aligned} \dim\left\{{}^{o}\boldsymbol{S}_{f,Leg}\right\} = {} & \dim\left({}^{a}\boldsymbol{S}_{f,Leg}\right) + \dim\left\{{}^{l}\boldsymbol{S}_{f,Leg}\right\} + \dim\left\{{}^{r}\boldsymbol{S}_{f,Leg}\right\} \\ & - \dim\left(\bigcap_{\mathrm{m}=a,l}\left\{{}^{\mathrm{m}}\boldsymbol{S}_{f,Leg}\right\}\right) - \dim\left(\bigcap_{\mathrm{m}=a,r}\left\{{}^{\mathrm{m}}\boldsymbol{S}_{f,Leg}\right\}\right) \\ & - \dim\left(\bigcap_{\mathrm{m}=l,r}\left\{{}^{\mathrm{m}}\boldsymbol{S}_{f,Leg}\right\}\right) + \dim\left(\bigcap_{\mathrm{m}=a,l,r}\left\{{}^{\mathrm{m}}\boldsymbol{S}_{f,Leg}\right\}\right). \end{aligned} \tag{5}$$

According to Eqs. (4) and (5), number synthesis results are finally discussed in Table 1. For simplicity, No. 1−3 just list three cases that there is no common motion between 3R and 2R1T. No. 4−17 shows all cases with at least one common motion among three modes. Number correlations on common finite motion, DOFs, motors, buffering dampers, limbs, etc. of ReLML are further discussed:

(1) To meet the output DOFs, there should arrange three motors in adjusting and roving modes, and three buffering dampers in landing mode. For a reasonable layout, it should adopt three metamorphic limbs with each limb having one buffering damper and two actuated joint axes.

(2) To simplify the multi-mode topology, the common motion between/among modes is required to be as more as possible. Otherwise, a complex topology requires more joints, limbs, or complex geometric constraints. Further, if the common motion has the dimension greater than or equal to one, then it must be continuous with constant direction and position in some reference frame.

Table 1 Number synthesis of multi-mode output motions

No.	$\bigcap_{\mathrm{m}=a,l}\{{}^{\mathrm{m}}S\}$	$\bigcap_{\mathrm{m}=a,r}\{{}^{\mathrm{m}}S\}$	$\bigcap_{\mathrm{m}=l,r}\{{}^{\mathrm{m}}S\}$	$\bigcap_{\mathrm{m}=a,l,r}\{{}^{\mathrm{m}}S\}$	$\{{}^{o}S\}$
1	0	0	1	0	8
2	0	0	2	0	7
3	0	0	3	0	6
4	1	1	1	1	7
5	1	1	2	1	6
6	1	1	3	1	5
7	1	2	1	1	6
8	1	2	2	1	5
9	1	2	3	1	4
10	2	1	1	1	6
11	2	1	2	1	5
12	2	1	3	1	4
13	2	2	1	1	5
14	2	2	2	1	4
15	2	2	2	2	5
16	2	2	3	1	3
17	2	2	3	2	4

4 Motion Representation and Switch Condition for Three-Mode Reconfiguration from Adjusting, Landing, to Roving

The finite motion of the source phase or any mode is generated by the intersection operation for the kinematic bonds of all metamorphic limbs ${}^{\mathrm{m}}\boldsymbol{S}_{f,L_j}$, written as:

$$\left\{{}^{\mathrm{m}}\boldsymbol{S}_{f,Leg}\right\} = \bigcap_{j=1}^{3}\left\{{}^{\mathrm{m}}\boldsymbol{S}_{f,L_j}\right\},\ \mathrm{m} = o,a,l,r. \tag{6}$$

The finite motion submanifold of source phase is the union set of those of three modes. Further, the end-effector submanifold and limb bonds have the relationship:

$$\{{}^{o}\boldsymbol{S}_{f,Leg}\} = \{{}^{a}\boldsymbol{S}_{f,Leg}\} \cup \left\{{}^{l}\boldsymbol{S}_{f,Leg}\right\} \cup \{{}^{r}\boldsymbol{S}_{f,Leg}\} = \left(\bigcap_{j=1}^{3}\left\{{}^{a}\boldsymbol{S}_{f,L_j}\right\}\right) \cup \left(\bigcap_{j=1}^{3}\left\{{}^{l}\boldsymbol{S}_{f,L_j}\right\}\right) \cup \left(\bigcap_{j=1}^{3}\left\{{}^{r}\boldsymbol{S}_{f,L_j}\right\}\right). \tag{7}$$

The finite motion of overall lander can be obtained by the equivalent mechanism model method. In adjusting mode that the ReLML hovering in the sky, four legs and main body construct a collaborative topology, there is no relative motion between body and environment; in landing and roving modes, four legs with body and environment construct a parallel topology, so the finite motion of overall lander is the intersection set of four legs' submanifolds.

$$\{{}^{\mathfrak{m}}\boldsymbol{S}_{f,Body}\} = \begin{cases} \emptyset & \mathfrak{m} = a, \\ \bigcap_{k=1}^{4}\{{}^{\mathfrak{m}}\boldsymbol{S}_{f,Leg_k}\} & \mathfrak{m} = l, r. \end{cases} \tag{8}$$

Mode switch and topology reconfiguration happens when changing the leg end-effector submanifold at the common configuration space—called the configuration transition space $\{\boldsymbol{CTS}\}$—between two adjacent operation modes. The ReLML has two types of switches with sequential occurrences, Eq. (9) shows the switch condition from adjusting to landing modes, and Eq. (10) gives the switch condition from landing to roving modes. The configuration transition condition indicates two adjacent modes should have the same finite motion (posture).

$$\{\boldsymbol{CTS}\}_{a\to l} = \left\{\boldsymbol{S}_{f,Leg}\middle|{}^{a}\boldsymbol{S}_{f,Leg} = {}^{l}\boldsymbol{S}_{f,Leg},\ \{{}^{a}\boldsymbol{S}_{f,Leg}\} \neq \left\{{}^{l}\boldsymbol{S}_{f,Leg}\right\}\right\}, \tag{9}$$

$$\{\boldsymbol{CTS}\}_{l\to r} = \left\{\boldsymbol{S}_{f,Leg}\middle|{}^{l}\boldsymbol{S}_{f,Leg} = {}^{r}\boldsymbol{S}_{f,Leg},\ \left\{{}^{l}\boldsymbol{S}_{f,Leg}\right\} \neq \{{}^{r}\boldsymbol{S}_{f,Leg}\}\right\}. \tag{10}$$

Algebraic structures of leg's end-effector submanifold can easily derive the simplest standard limb bonds of three modes, which also share a partially common kinematic bond. After comparison, the metamorphic joint bonds can be identified, they result in this study's particularity by the concurrence of active and passive metamorphoses. (1) The bond of active metamorphic axis-variable joint ${}^{m}R_{v}$ has three phases, including two orthogonal switchable rotations (directions $\boldsymbol{u}$ and $\boldsymbol{v}$, motor control) for adjusting and roving, and rigid connection for a reliable landing truss. (2) The bond of passive metamorphic buffering damper ${}^{m}P_{b}$ has two phases, i.e., the translation to absorb touchdown impact energy, and rigid connection in adjusting and roving modes.

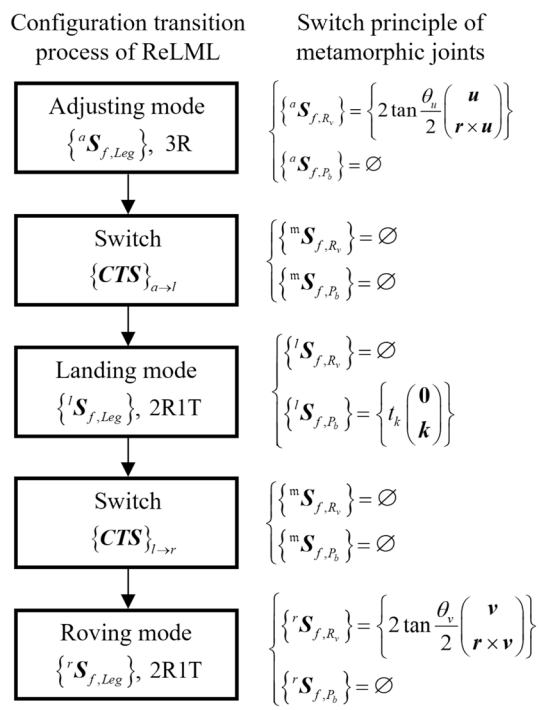

Figure 2 Configuration transition process of ReLML and switch principle of metamorphic joints

$$\{{}^{\mathfrak{m}}\boldsymbol{S}_{f,R_v}\} = \begin{cases} \left\{2\tan\frac{\theta_u}{2}\begin{pmatrix}\boldsymbol{u}\\ \boldsymbol{r}\times\boldsymbol{u}\end{pmatrix}\right\} & \mathfrak{m} = a, \\ \emptyset & \mathfrak{m} = l, \\ \left\{2\tan\frac{\theta_v}{2}\begin{pmatrix}\boldsymbol{v}\\ \boldsymbol{r}\times\boldsymbol{v}\end{pmatrix}\right\} & \mathfrak{m} = r, \end{cases} \tag{11}$$

$$\{{}^{\mathfrak{m}}\boldsymbol{S}_{f,P_b}\} = \begin{cases} \emptyset & \mathfrak{m} = a, r, \\ \left\{t_k\begin{pmatrix}\boldsymbol{0}\\ \boldsymbol{k}\end{pmatrix}\right\} & \mathfrak{m} = l, \end{cases}$$

where $\boldsymbol{u}$ is orthogonal to main body to guarantee reliable landing impact transfer flow after any adjusting pose. $\boldsymbol{v}$ is parallel to main body. $\boldsymbol{k}$ is the translation direction of ${}^{m}P_{b}$.

Switch principle of metamorphic joints corresponding to the configuration transition process of ReLML are illustrated in Figure 2. The metamorphic essence is the change of end-effector submanifold through $\{\boldsymbol{CTS}\}$. The switch principle of active and passive metamorphic joints is to produce various geometric constraints for the corresponding operation modes.

5 Topology Synthesis of Metamorphic Execution Mechanism for Adjusting, Landing, Roving

5.1 Determine Kinematic Bond of Metamorphic Limb

According to Eqs. (6) and (7), the source metamorphic limb bond should contain the union sets of three modes' finite motions, indicating the motions of the

minimum-dimension limb is identical with metamorphic execution mechanism.

$$\left\{{}^{o}\boldsymbol{S}_{f,L_j}\right\} \supseteq \left\{{}^{o}\boldsymbol{S}_{f,Leg}\right\} = \left\{{}^{a}\boldsymbol{S}_{f,Leg}\right\} \cup \left\{{}^{l}\boldsymbol{S}_{f,Leg}\right\} \cup \left\{{}^{r}\boldsymbol{S}_{f,Leg}\right\}. \tag{12}$$

Four source bond families are classified by dimensions. Notably, this paper does not consider that containing translation factor for practical purpose, besides ${}^{\mathrm{m}}\mathrm{P}_{\mathrm{b}}$.

(1) Family 1: $\dim\{{}^{\mathrm{m}}\boldsymbol{S}_{f,L_j}\} = 3$. The metamorphic bond in each mode always generates 3D finite motions, i.e., 3R and double 2R1T. Given $\dim\{{}^{\mathrm{m}}\boldsymbol{S}_{f,L_j}\} = \dim\{{}^{\mathrm{m}}\boldsymbol{S}_{f,Leg}\} = 3$ is satisfied in each mode, all constraints on moving platform are supplied by this limb bond. Thus, the mechanism among three modes must have two common continuous rotations and one unique continuous rotation or translation. In other words, the source bond contains three rotation and two translation factors, $\dim\{{}^{o}\boldsymbol{S}_{f,L_j}\} = 5$. Thereinto, one translation factor for roving should be replaced by two parallel rotations. Three types are as follows.

The first type of source bond is the union set of adjusting motion in Eq. (1), landing and roving motions in the first subequation and derivative type of Eq. (2). The finite screw format defined by the triangle product is further derived from the manifold operations (multiplication and union) to reveal the motion generation within three modes.

$$\begin{aligned}
&\left\{{}^{o}\boldsymbol{S}_{f,L_j,11}\right\} = \left\{{}^{a}\boldsymbol{S}_{f,Leg}\right\} \cup \left\{{}^{l}\boldsymbol{S}_{f,Leg,(1)}\right\} \cup \left\{{}^{r}\boldsymbol{S}_{f,Leg,(1)}\right\} \\
&= \left(\left\{2\tan\frac{\theta_{a1}}{2}\begin{pmatrix}\boldsymbol{u}\\ \boldsymbol{r}_{a1}\times\boldsymbol{u}\end{pmatrix}\right\} \cup \left\{2\tan\frac{\theta_{r1}}{2}\begin{pmatrix}\boldsymbol{v}\\ \boldsymbol{r}_{r1}\times\boldsymbol{v}\end{pmatrix}\right\} \cup \left\{t_{l1}\begin{pmatrix}\boldsymbol{0}\\ \boldsymbol{k}\end{pmatrix}\right\}\right) \\
&\quad \cdot \left\{2\tan\frac{\theta_{a2}}{2}\begin{pmatrix}\boldsymbol{v}\\ \boldsymbol{r}_{a2}\times\boldsymbol{v}\end{pmatrix}\right\}\left\{2\tan\frac{\theta_{a3}}{2}\begin{pmatrix}\boldsymbol{w}\\ \boldsymbol{r}_{a3}\times\boldsymbol{w}\end{pmatrix}\right\} \\
&\Rightarrow {}^{o}\boldsymbol{S}_{f,L_j,11} = 2\tan\frac{\theta_4}{2}\begin{pmatrix}\boldsymbol{w}\\ \boldsymbol{r}_3\times\boldsymbol{w}\end{pmatrix}\Delta 2\tan\frac{\theta_3}{2}\begin{pmatrix}\boldsymbol{v}\\ \boldsymbol{r}_3\times\boldsymbol{v}\end{pmatrix} \\
&\quad \Delta\left(t_k\begin{pmatrix}\boldsymbol{0}\\ \boldsymbol{k}\end{pmatrix}\right)_{P_b}\Delta\left(2\tan\frac{\theta_2}{2}\begin{pmatrix}\boldsymbol{v}\\ \boldsymbol{r}_1\times\boldsymbol{v}\end{pmatrix}\Delta 2\tan\frac{\theta_1}{2}\begin{pmatrix}\boldsymbol{u}\\ \boldsymbol{r}_1\times\boldsymbol{u}\end{pmatrix}\right)_{R_v},
\end{aligned} \tag{13}$$

where N_f and N_t are family and type numbers of ${}^{o}\boldsymbol{S}_{f,L_j,N_fN_t}$ respectively, $\bar{\boldsymbol{s}}$ is the unit direction vector of continuous motion. $\boldsymbol{u} = \bar{\boldsymbol{s}}_{a1}$, $\boldsymbol{v} = \bar{\boldsymbol{s}}_{a2} = \bar{\boldsymbol{s}}_{l2} = \bar{\boldsymbol{s}}_{r1} = \bar{\boldsymbol{s}}_{r2}$, $\boldsymbol{w} = \bar{\boldsymbol{s}}_{a3} = \bar{\boldsymbol{s}}_{l3} = \bar{\boldsymbol{s}}_{r3}$, $\boldsymbol{k} = \bar{s}_{l1}$, $\boldsymbol{r}_1 = \boldsymbol{r}_{a1} = \boldsymbol{r}_{r1}$, $\boldsymbol{r}_3 = \boldsymbol{r}_{a2} = \boldsymbol{r}_{a3} = \boldsymbol{r}_{l2} = \boldsymbol{r}_{l3} = \boldsymbol{r}_{r2} = \boldsymbol{r}_{r3}$.

The second type is united by the adjusting motion in Eq. (3), landing and roving motions in the second subequation and derivative type of Eq. (2).

$$\begin{aligned}
&\left\{{}^{o}\boldsymbol{S}_{f,L_j,12}\right\} = \left\{{}^{a}\boldsymbol{S}_{f,Leg}\right\} \cup \left\{{}^{l}\boldsymbol{S}_{f,Leg,(2)}\right\} \cup \left\{{}^{r}\boldsymbol{S}_{f,Leg,(2)}\right\} \\
&= \left(\left\{2\tan\frac{\theta_{a1}}{2}\begin{pmatrix}\boldsymbol{u}\\ \boldsymbol{r}_{a1}\times\boldsymbol{u}\end{pmatrix}\right\} \cup \left\{2\tan\frac{\theta_{r1}}{2}\begin{pmatrix}\boldsymbol{v}\\ \boldsymbol{r}_{r1}\times\boldsymbol{v}\end{pmatrix}\right\}\right) \\
&\quad \cdot \left\{2\tan\frac{\theta_{a2}}{2}\begin{pmatrix}\boldsymbol{v}\\ \boldsymbol{r}_{a2}\times\boldsymbol{v}\end{pmatrix}\right\}\left(\cup\left\{t_{l2}\begin{pmatrix}\boldsymbol{0}\\ \boldsymbol{k}\end{pmatrix}\right\}\right) \cdot \left\{2\tan\frac{\theta_{a3}}{2}\begin{pmatrix}\boldsymbol{w}\\ \boldsymbol{r}_{a3}\times\boldsymbol{w}\end{pmatrix}\right\} \\
&\Rightarrow {}^{o}\boldsymbol{S}_{f,L_j,12} = 2\tan\frac{\theta_4}{2}\begin{pmatrix}\boldsymbol{w}\\ \boldsymbol{r}_4\times\boldsymbol{w}\end{pmatrix}\Delta\left(t_k\begin{pmatrix}\boldsymbol{0}\\ \boldsymbol{k}\end{pmatrix}\right)_{P_b}\Delta 2\tan\frac{\theta_3}{2}\begin{pmatrix}\boldsymbol{v}\\ \boldsymbol{r}_3\times\boldsymbol{v}\end{pmatrix} \\
&\quad \Delta\left(2\tan\frac{\theta_2}{2}\begin{pmatrix}\boldsymbol{v}\\ \boldsymbol{r}_1\times\boldsymbol{v}\end{pmatrix}\Delta 2\tan\frac{\theta_1}{2}\begin{pmatrix}\boldsymbol{u}\\ \boldsymbol{r}_1\times\boldsymbol{u}\end{pmatrix}\right)_{R_v},
\end{aligned} \tag{14}$$

where $\boldsymbol{u} = \bar{\boldsymbol{s}}_{a1}$, $\boldsymbol{v} = \bar{\boldsymbol{s}}_{a2} = \bar{\boldsymbol{s}}_{l1} = \bar{\boldsymbol{s}}_{r1}$, $\boldsymbol{w} = \bar{\boldsymbol{s}}_{a3} = \bar{\boldsymbol{s}}_{l3} = \bar{\boldsymbol{s}}_{r3}$, $\boldsymbol{k} = \bar{\boldsymbol{s}}_{l2}$, and $\boldsymbol{r}_1 = \boldsymbol{r}_{a1} = \boldsymbol{r}_{r1}$, $\boldsymbol{r}_3 = \boldsymbol{r}_{a2} = \boldsymbol{r}_{l1} = \boldsymbol{r}_{r2}$, $\boldsymbol{r}_4 = \boldsymbol{r}_{a3} = \boldsymbol{r}_{l3} = \boldsymbol{r}_{r3}$.

The third type is united by adjusting motion in Eq. (1), landing motion in the third subequation of Eq. (2), and roving motion in the first derivative type.

$$
\begin{aligned}
&\left\{{}^{o}\boldsymbol{S}_{f,L_j,13}\right\} = \left\{{}^{a}\boldsymbol{S}_{f,Leg}\right\} \cup \left\{{}^{l}\boldsymbol{S}_{f,Leg,(3)}\right\} \cup \left\{{}^{r}\boldsymbol{S}_{f,Leg,(1)}\right\} \\
&= \left(\left\{2\tan\frac{\theta_{a1}}{2}\begin{pmatrix}\boldsymbol{u}\\ \boldsymbol{r}_{a1}\times\boldsymbol{u}\end{pmatrix}\right\} \cup \left\{2\tan\frac{\theta_{r1}}{2}\begin{pmatrix}\boldsymbol{v}\\ \boldsymbol{r}_{r1}\times\boldsymbol{v}\end{pmatrix}\right\}\right) \\
&\quad \cdot \left\{2\tan\frac{\theta_{a2}}{2}\begin{pmatrix}\boldsymbol{v}\\ \boldsymbol{r}_{a2}\times\boldsymbol{v}\end{pmatrix}\right\}\left\{2\tan\frac{\theta_{a3}}{2}\begin{pmatrix}\boldsymbol{w}\\ \boldsymbol{r}_{a3}\times\boldsymbol{w}\end{pmatrix}\right\} \cup \left(\left\{t_{l3}\begin{pmatrix}\boldsymbol{0}\\ \boldsymbol{k}\end{pmatrix}\right\}\right) \\
&\Rightarrow {}^{o}\boldsymbol{S}_{f,L_j,13} = \left(t_k\begin{pmatrix}\boldsymbol{0}\\ \boldsymbol{k}\end{pmatrix}\right)_{P_b} \Delta 2\tan\frac{\theta_4}{2}\begin{pmatrix}\boldsymbol{w}\\ \boldsymbol{r}_3\times\boldsymbol{w}\end{pmatrix} \Delta 2\tan\frac{\theta_3}{2}\begin{pmatrix}\boldsymbol{v}\\ \boldsymbol{r}_3\times\boldsymbol{v}\end{pmatrix} \\
&\quad \Delta\left(2\tan\frac{\theta_2}{2}\begin{pmatrix}\boldsymbol{v}\\ \boldsymbol{r}_1\times\boldsymbol{v}\end{pmatrix} \Delta 2\tan\frac{\theta_1}{2}\begin{pmatrix}\boldsymbol{u}\\ \boldsymbol{r}_1\times\boldsymbol{u}\end{pmatrix}\right)_{R_v},
\end{aligned}
\tag{15}
$$

where $\boldsymbol{u} = \bar{\boldsymbol{s}}_{a1}$, $\boldsymbol{v} = \bar{\boldsymbol{s}}_{a2} = \bar{\boldsymbol{s}}_{l1} = \bar{\boldsymbol{s}}_{r1}$, $\boldsymbol{w} = \bar{\boldsymbol{s}}_{a3} = \bar{\boldsymbol{s}}_{l2} = \bar{\boldsymbol{s}}_{r3}$, $\boldsymbol{k} = \bar{\boldsymbol{s}}_{l3}$, and $\boldsymbol{r}_1 = \boldsymbol{r}_{a1} = \boldsymbol{r}_{r1}$, $\boldsymbol{r}_3 = \boldsymbol{r}_{a2} = \boldsymbol{r}_{a3} = \boldsymbol{r}_{l1} = \boldsymbol{r}_{l2} = \boldsymbol{r}_{r2} = \boldsymbol{r}_{r3}$.

(2) Family 2: $\dim\{{}^{m}\boldsymbol{S}_{f,L_j}\} = 4$. The metamorphic limb bond in each mode always generates 4D finite motion containing at least two independent rotations. This family allows the non-continuous finite rotations in three modes that can form a general two- or three-order system, which means the direction and even position of motion axis can be variable with respect to pose. The source bond is generated by six motion factors, i.e., $\dim\{{}^{o}\boldsymbol{S}_{f,L_j}\} = 6$. Three feasible types are obtained by adding a rotation factor to left side of Eqs. (13)–(15), so axis coincidence conditions in family 1 are unneces-

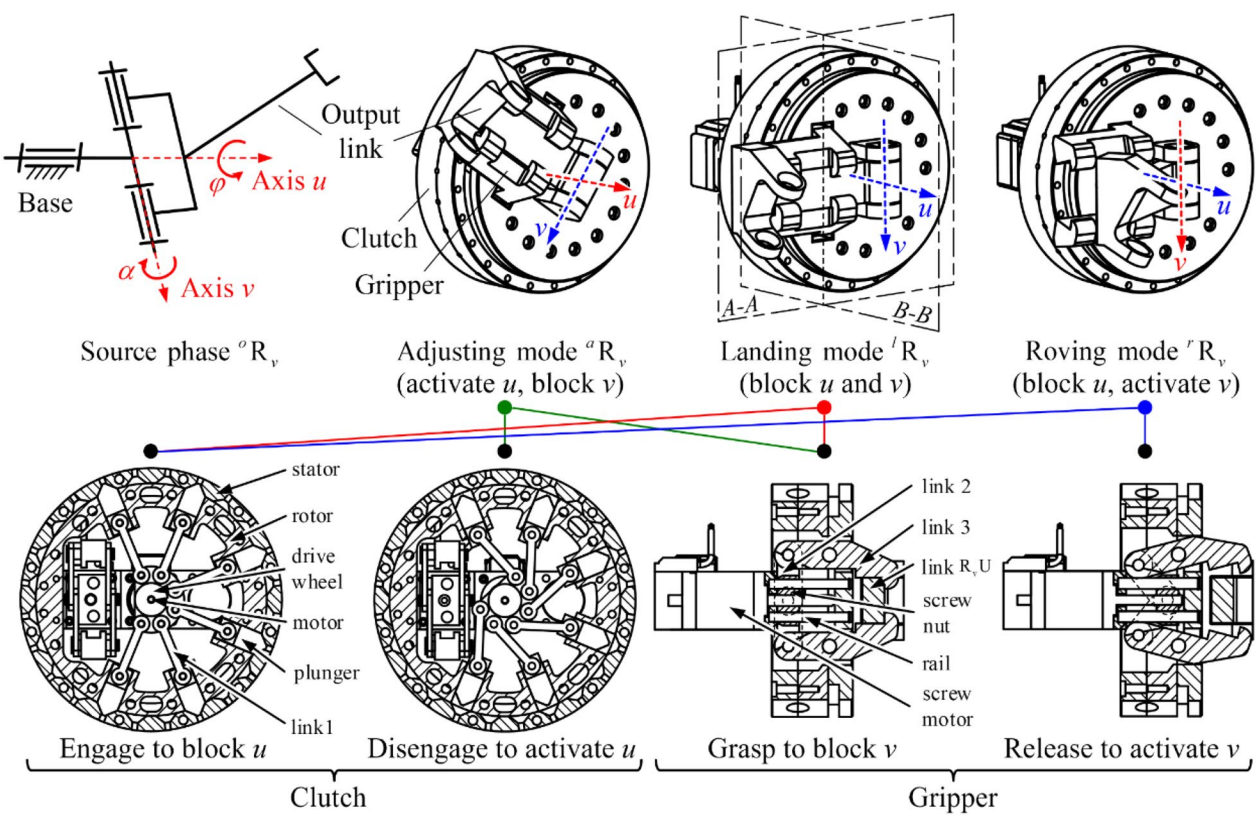

Figure 3 Structure of metamorphic variable-axis joint ${}^{m}R_v$: source phase, operation modes, and drive process

sary. Here shows the finite screw form directly. The first type offers a revolute-planar-spherical bond with the first revolute axis and spherical center in a plane.

$$ {}^{o}\boldsymbol{S}_{f,L_j,21} = 2\tan\frac{\theta_5}{2}\begin{pmatrix}\boldsymbol{k}\\ \boldsymbol{r}_3\times\boldsymbol{k}\end{pmatrix}\Delta^{o}\boldsymbol{S}_{f,L_j,11}. \quad (16)$$

The second type provides a revolute-planar-universal bond with the revolute axis and universal center in the plane, see Eq. (17). The third type is also given by Eq. (18).

$$ {}^{o}\boldsymbol{S}_{f,L_j,22} = 2\tan\frac{\theta_5}{2}\begin{pmatrix}\boldsymbol{v}\\ \boldsymbol{r}_4\times\boldsymbol{v}\end{pmatrix}\Delta^{o}\boldsymbol{S}_{f,L_j,12}, \quad (17)$$

$$ {}^{o}\boldsymbol{S}_{f,L_j,23} = 2\tan\frac{\theta_5}{2}\begin{pmatrix}\boldsymbol{k}\\ \boldsymbol{r}_3\times\boldsymbol{k}\end{pmatrix}\Delta^{o}\boldsymbol{S}_{f,L_j,13}. \quad (18)$$

Similar steps derive Family 3 with $\dim\{{}^{\mathrm{m}}\boldsymbol{S}_{f,L_j}\} = 5$ and Family 4 with $\dim\{{}^{\mathrm{m}}\boldsymbol{S}_{f,L_j}\} = 6$, which allow to produce the general two- or three-order system of non-continuous finite rotations for constructing a broader mechanism family.

$$ {}^{o}\boldsymbol{S}_{f,L_j,31} = 2\tan\frac{\theta_6}{2}\begin{pmatrix}\boldsymbol{w}\\ \boldsymbol{r}_6\times\boldsymbol{w}\end{pmatrix}\Delta^{o}\boldsymbol{S}_{f,L_j,21},$$
$$ {}^{o}\boldsymbol{S}_{f,L_j,41} = 2\tan\frac{\theta_7}{2}\begin{pmatrix}\boldsymbol{s}\\ \boldsymbol{r}_6\times\boldsymbol{s}\end{pmatrix}\Delta 2\tan\frac{\theta_6}{2}\begin{pmatrix}\boldsymbol{w}\\ \boldsymbol{r}_6\times\boldsymbol{w}\end{pmatrix}\Delta^{o}\boldsymbol{S}_{f,L_j,21}, \quad (19)$$

$$ {}^{o}\boldsymbol{S}_{f,L_j,32} = 2\tan\frac{\theta_6}{2}\begin{pmatrix}\boldsymbol{s}\\ \boldsymbol{r}_4\times\boldsymbol{s}\end{pmatrix}\Delta^{o}\boldsymbol{S}_{f,L_j,22},$$
$$ {}^{o}\boldsymbol{S}_{f,L_j,42} = 2\tan\frac{\theta_7}{2}\begin{pmatrix}\boldsymbol{v}\\ \boldsymbol{r}_7\times\boldsymbol{v}\end{pmatrix}2\tan\frac{\theta_6}{2}\begin{pmatrix}\boldsymbol{s}\\ \boldsymbol{r}_4\times\boldsymbol{s}\end{pmatrix}\Delta^{o}\boldsymbol{S}_{f,L_j,32}, \quad (20)$$

$$ {}^{o}\boldsymbol{S}_{f,L_j,33} = 2\tan\frac{\theta_6}{2}\begin{pmatrix}\boldsymbol{w}\\ \boldsymbol{r}_6\times\boldsymbol{w}\end{pmatrix}\Delta^{o}\boldsymbol{S}_{f,L_j,23},$$
$$ {}^{o}\boldsymbol{S}_{f,L_j,43} = 2\tan\frac{\theta_7}{2}\begin{pmatrix}\boldsymbol{s}\\ \boldsymbol{r}_6\times\boldsymbol{s}\end{pmatrix}\Delta 2\tan\frac{\theta_6}{2}\begin{pmatrix}\boldsymbol{w}\\ \boldsymbol{r}_6\times\boldsymbol{w}\end{pmatrix}{}^{o}\boldsymbol{S}_{f,L_j,33}. \quad (21)$$

5.2 Design Mechanical Generator of Metamorphic Limb

Mechanical generators and actuation/deformation of metamorphic joints are first argued. Targeted to high reliability in aerospace engineering, the mechanical generator should be installed on main body, so the complex structures are excluded directly. The buffering damper ${}^{\mathrm{m}}\mathrm{P}_{\mathrm{b}}$ is a mature technology validated in Chang'E project [8], its deformation process stems from the embedded aluminum honeycomb structure through a large touch-down impact, and produces a large-scale buffering configuration variation. The variable-axis joint ${}^{\mathrm{m}}\mathrm{R}_{\mathrm{v}}$ requires to be designed, its final structure and drive process are illustrated in Figure 3: (1) The clutch mechanism aims to block or activate axis u, utilizing six units of planar RRRP mechanisms in a circular array to enhance strength and reliability. It has one-input six-output property, all units are driven by the same motor. The engaged state to block

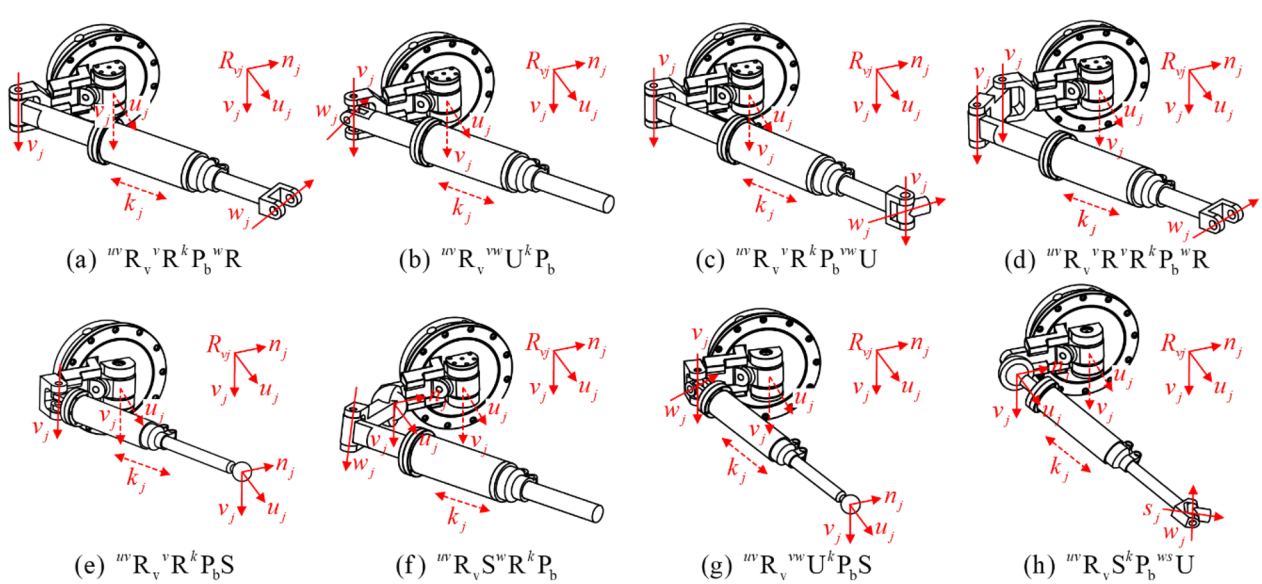

Figure 4 Typical structures of metamorphic limbs: **a**, **b** Family 1, **c**, **d** Family 2, **e**, **f** Family 3, **g**, **h** Family 4

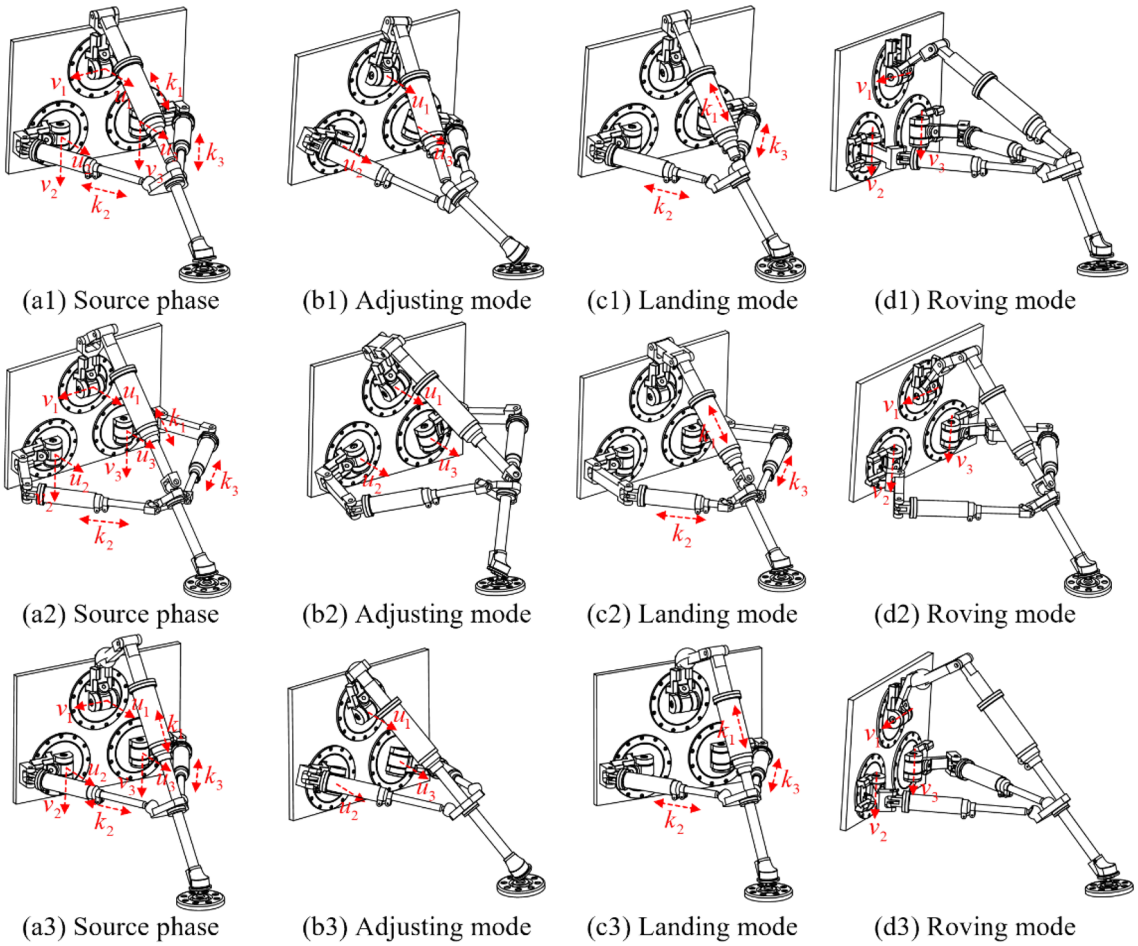

Figure 5 Subcategory 5-5-5: **a1–d1** $3^{uv}R_v{}^{v}R^{k}P_b S$, **a2–d2** $3^{uv}R_v{}^{v}R^{v}R^{k}P_b{}^{ws}U$, **a3–d3** $^{uv}R_v S^{w}R^{k}P_b \& 2^{uv}R_v{}^{v}R^{k}P_b S$

axis u occurs when the plunger falls into the stator bore and achieves the dead point, so the clutch also has a great force-amplifier property. The disengaged state to activate axis u occurs when the plunger returns back to the rotor. (2) The gripper mechanism aims to grasp or release axis v, by two units of planar PRRR mechanisms in a symmetrical array for better strength and reliability. Both units are driven by the same motor, so the gripper has single-input double-output property. Its grasped state to block axis v occurs when link 3 grasps the output link, meantime, link 2 is perpendicular to the screw motor axis. The dead point is achieved for better force-resisting property, especially taking effects for touchdown impact. The released state to activate axis v occurs when there is no contact between link 3 and output link.

According to Eqs. (13)–(15), the standard structures of family 1 in source phase are $^{uv}R_v{}^{k}P_b{}^{vw}U$, $^{uv}R_v{}^{v}R^{k}P_b{}^{w}R$, $^{uv}R_v{}^{vw}U^{k}P_b$. Each provides two common continuous finite rotations among three modes, and one unique continuous rotation/translation in mode. After applying screw triangle product, two derivative structures can be obtained by joint type and location substitutions: $^{uv}R_v{}^{v}C_b{}^{w}R$ and $^{uv}R_v{}^{v}R^{w}C_b$, where $^{w}C_b$ is a new metamorphic cylindrical joint made up of buffering damper and revolute joint arranged co-axially.

Based on Eqs. (16)–(18), the standard structures of family 2 are $^{uv}R_v{}^{k}P_b S$, $^{uv}R_v{}^{v}R^{k}P_b{}^{vw}U$, $^{uv}R_v S^{k}P_b$. Operating screw triangle product, five derivative ones are $^{uv}R_v{}^{k}C_b{}^{vw}U$, $^{uv}R_v{}^{k}P_b{}^{v}R^{vw}U$, $^{uv}R_v{}^{v}R^{v}R^{k}C_b$, $^{uv}R_v{}^{v}R^{v}R^{k}P_b{}^{w}R$, $^{uv}R_v{}^{vw}U^{k}C_b$. Employing similar procedures based on Eqs. (19)–(21), we can also obtain the source metamorphic limb structures of family 3: $^{uv}R_v{}^{k}P_b S^{w}R$, $^{uv}R_v{}^{v}R^{k}P_b S$, $^{uv}R_v S^{k}P_b{}^{w}R$, $^{uv}R_v{}^{k}C_b{}^{vw}U^{w}R$, $^{uv}R_v{}^{v}R^{v}R^{k}P_b{}^{ws}U$, $^{uv}R_v{}^{v}R^{v}R^{k}C_b{}^{s}R$, $^{uv}R_v{}^{k}P_b{}^{v}RS$, $^{uv}R_v{}^{vw}U^{k}C_b{}^{w}R$, $^{uv}R_v S^{w}R^{k}P_b$, $^{uv}R_v{}^{vk}U^{k}P_b{}^{w}R^{w}R$; and those of family 4: $^{uv}R_v{}^{k}P_b S^{ws}U$, $^{uv}R_v{}^{v}R^{k}P_b S^{v}R$, $^{uv}R_v S^{k}P_b{}^{ws}U$, $^{uv}R_v{}^{k}P_b{}^{vw}US$, $^{uv}R_v{}^{k}C_b{}^{w}RS$, $^{uv}R_v{}^{k}P_b{}^{v}RS^{v}R$, $^{uv}R_v{}^{vw}U^{k}P_b S$, $^{uv}R_v S^{w}R^{k}C_b$.

For brevity, we here take ${}^{o}\boldsymbol{S}_{f,L_j,32}$ as an example to show the calculation process of derivative structures, see Eq. (22): Firstly, (a) derives the structure $^{uv}R_v{}^{v}R^{v}R^{k}P_b{}^{ws}U$ from

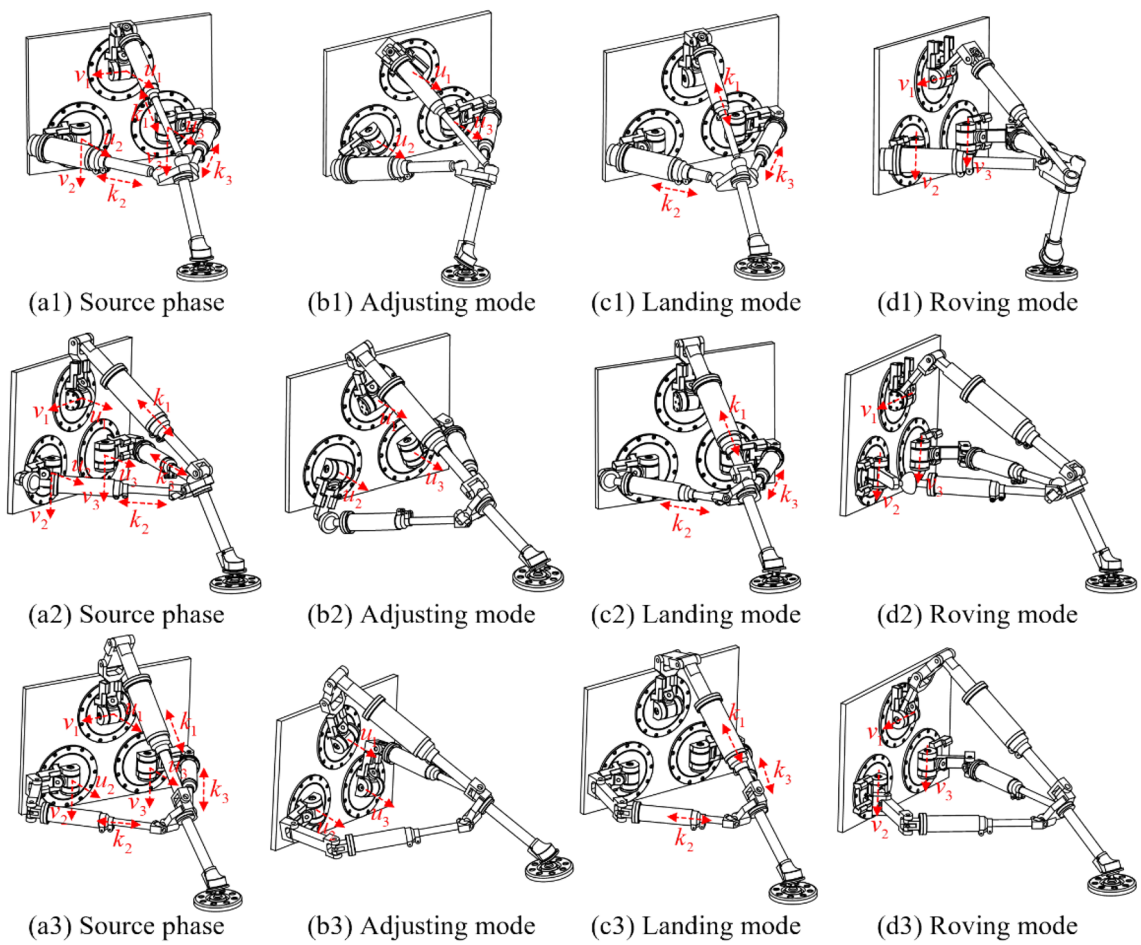

Figure 6 Subcategory 4-5-6: **a1–d1** $^{uv}R_v{}^kP_bS\&^{uv}R_v{}^vR^kP_bS\&^{uv}R_v{}^{vw}U^kP_bS$, **a2–d2** $^{uv}R_v{}^vR^kP_b{}^{vw}U\&^{uv}R_v{}^vR^kP_bS\&^{uv}R_vS^kP_b{}^{ws}U$, **a3–d3** $^{uv}R_v{}^vR^vR^kP_b{}^wR\&^{uv}R_v{}^vR^vR^kP_b{}^{ws}U\&^{uv}R_v{}^{vw}U^kP_bS$

Eq. (20) by joint location substitution; then, (b) derives $^{uv}R_v{}^vR^vR^kC_b{}^sR$ by joint type substitution when assigning $\boldsymbol{w}=\boldsymbol{k}$; finally, (c) obtains $^{uv}R_v{}^kP_b{}^vRS$ by changing the positions of joints following closure and equivalence.

The above source metamorphic limb structures are synthesized in the limb frame R_{vj}-$u_jv_jn_j$. For brevity, Figure 4 illustrates two typical ones of each family.

$$
\begin{aligned}
{}^o\boldsymbol{S}_{f,L_j32} &= \left(2\tan\frac{\theta_6}{2}\begin{pmatrix}\boldsymbol{s}\\ \boldsymbol{r}_4\times\boldsymbol{s}\end{pmatrix}\Delta 2\tan\frac{\theta_5}{2}\begin{pmatrix}\boldsymbol{w}\\ \boldsymbol{r}_4\times\boldsymbol{w}\end{pmatrix}\right)_U \Delta\left(t_k\begin{pmatrix}\boldsymbol{0}\\ \boldsymbol{k}\end{pmatrix}\right)_{P_b}\\
&\quad \Delta 2\tan\frac{\theta_4}{2}\begin{pmatrix}\boldsymbol{v}\\ (\boldsymbol{r}_4+t_k\boldsymbol{k})\times\boldsymbol{v}\end{pmatrix}\Delta 2\tan\frac{\theta_3}{2}\begin{pmatrix}\boldsymbol{v}\\ \boldsymbol{r}_3\times\boldsymbol{v}\end{pmatrix}\Delta\,{}^o\boldsymbol{S}_{f,R_v},\ \text{(a)}\\
&= 2\tan\frac{\theta_6}{2}\begin{pmatrix}\boldsymbol{s}\\ \boldsymbol{r}_4\times\boldsymbol{s}\end{pmatrix}\Delta\left(2\tan\frac{\theta_5}{2}\begin{pmatrix}\boldsymbol{k}\\ \boldsymbol{r}_4\times\boldsymbol{k}\end{pmatrix}+t_k\begin{pmatrix}\boldsymbol{0}\\ \boldsymbol{k}\end{pmatrix}\right)_{C_b}\\
&\quad \Delta 2\tan\frac{\theta_4}{2}\begin{pmatrix}\boldsymbol{v}\\ (\boldsymbol{r}_4+t_k\boldsymbol{k})\times\boldsymbol{v}\end{pmatrix}\Delta 2\tan\frac{\theta_3}{2}\begin{pmatrix}\boldsymbol{v}\\ \boldsymbol{r}_3\times\boldsymbol{v}\end{pmatrix}\Delta\,{}^o\boldsymbol{S}_{f,R_v},\ \text{(b)}\\
&= \left(2\tan\frac{\theta_6}{2}\begin{pmatrix}\boldsymbol{s}\\ \boldsymbol{r}_4\times\boldsymbol{s}\end{pmatrix}\Delta 2\tan\frac{\theta_5}{2}\begin{pmatrix}\boldsymbol{w}\\ \boldsymbol{r}_4\times\boldsymbol{w}\end{pmatrix}\Delta 2\tan\frac{\theta_4}{2}\begin{pmatrix}\boldsymbol{v}\\ \boldsymbol{r}_4\times\boldsymbol{v}\end{pmatrix}\right)_S\\
&\quad \Delta 2\tan\frac{\theta_3}{2}\begin{pmatrix}\boldsymbol{v}\\ \boldsymbol{r}_3\times\boldsymbol{v}\end{pmatrix}\Delta\left(t_k\begin{pmatrix}\boldsymbol{0}\\ \exp(\theta_3\tilde{\boldsymbol{v}})\boldsymbol{k}\end{pmatrix}\right)_{P_b}\Delta\,{}^o\boldsymbol{S}_{f,R_v}.\ \text{(c)}
\end{aligned}
\tag{22}
$$

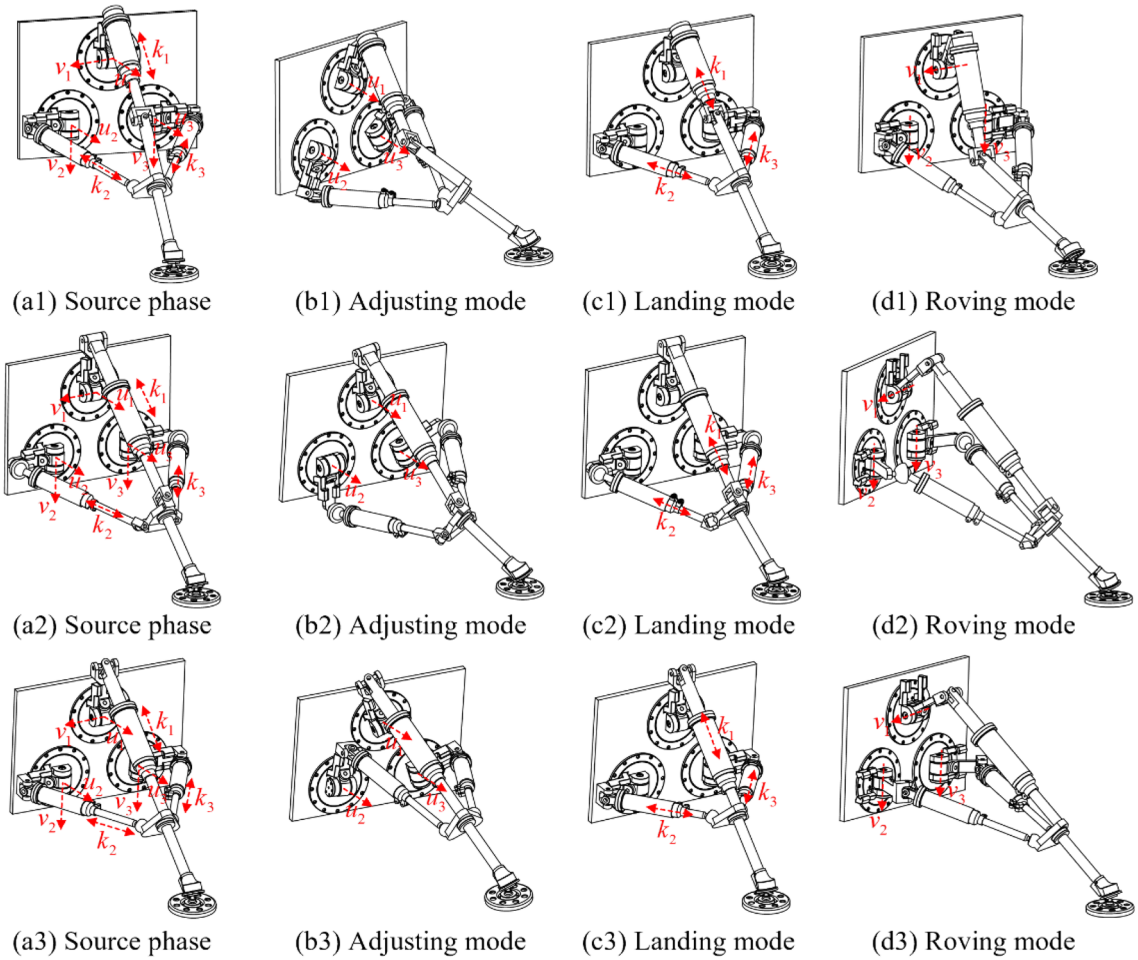

Figure 7 Subcategory 3-6-6: **a1–d1** $^{uv}R_v{}^kP_b{}^{vw}U\&2^{uv}R_v{}^{vw}U^kP_bS$, **a2–d2** $^{uv}R_v{}^vR^kP_b{}^wR\&2^{uv}R_vS^kP_b{}^{ws}U$, **a3–d3** $^{uv}R_v{}^{vw}U^kP_b\&2^{uv}R_v{}^{vw}U^kP_bS$

Table 2 Topology synthesis results of subcategory 5-5-5

Type	Result		
1	$^{uv}R_v{}^kP_bS^wR\&$ $2^{uv}R_v{}^vR^kP_bS$	$^{uv}R_v{}^kC_b{}^{vw}U^wR\&$ $2^{uv}R_v{}^vR^kP_bS$	$^{uv}R_v{}^kP_bS^wR\&$ $2^{uv}R_v{}^kP_b{}^vRS$
	$^{uv}R_v{}^kC_b{}^{vw}U^wR\&$ $2^{uv}R_v{}^kP_b{}^vRS$	$^{uv}R_v{}^kP_bS^wR\&$ $^{uv}R_v{}^kP_b{}^vRS\&$ $^{uv}R_v{}^{vw}U^kC_b{}^wR$	$^{uv}R_v{}^kP_bS^wR\&$ $^{uv}R_v{}^kP_b{}^vRS\&$ $^{uv}R_vS^wR^kP_b$
2	$3^{uv}R_v{}^vR^kP_bS$	$3^{uv}R_v{}^vR^vR^kP_b{}^{ws}U$	$3^{uv}R_v{}^vR^vR^kC_b{}^sR$
	$3^{uv}R_v{}^kP_b{}^vRS$	$^{uv}R_v{}^kP_b{}^vRS\&$ $2^{uv}R_v{}^vR^kP_bS$	$^{uv}R_v{}^vR^kP_bS\&$ $2^{uv}R_v{}^kP_b{}^vRS$
	$^{uv}R_v{}^vR^kP_bS\&$ $^{uv}R_v{}^kP_b{}^vRS\&$ $^{uv}R_v{}^kP_bS^wR$	$^{uv}R_v{}^vR^kP_bS\&$ $^{uv}R_v{}^kP_b{}^vRS\&$ $^{uv}R_v{}^kC_b{}^{vw}U^wR$	$^{uv}R_v{}^vR^kP_bS\&$ $^{uv}R_v{}^kP_b{}^vRS\&$ $^{uv}R_vS^kP_b{}^wR$
3	$^{uv}R_vS^wR^kP_b\&$ $2^{uv}R_v{}^vR^kP_bS$	$^{uv}R_vS^kP_b{}^wR\&$ $2^{uv}R_v{}^vR^kP_bS$	$^{uv}R_v{}^{vw}U^kC_b{}^wR\&$ $2^{uv}R_v{}^vR^kP_bS$
	$^{uv}R_vS^kP_b{}^wR\&$ $2^{uv}R_v{}^kP_b{}^vRS$	$^{uv}R_v{}^{vw}U^kC_b{}^wR\&$ $2^{uv}R_v{}^kP_b{}^vRS$	$^{uv}R_vS^wR^kP_b\&$ $2^{uv}R_v{}^kP_b{}^vRS$

Table 3 Topology synthesis results of subcategory 4-5-6

Type	Result		
1	$^{uv}R_v{}^kP_bS\&$ $^{uv}R_v{}^vR^kP_bS\&$ $^{uv}R_v{}^{vw}U^kP_bS$	$^{uv}R_v{}^kP_bS\&$ $^{uv}R_v{}^vR^vR^kP_b{}^{ws}U$ $\&^{uv}R_v{}^kP_bS^{ws}U$	$^{uv}R_v{}^kP_bS\&$ $^{uv}R_v{}^vR^vR^kC_b{}^sR\&$ $^{uv}R_v{}^vR^kP_bS^vR$
	$^{uv}R_v{}^kP_bS\&$ $^{uv}R_v{}^kP_b{}^vRS\&$ $^{uv}R_vS^kP_b{}^{ws}U$	$^{uv}R_v{}^kP_bS\&$ $^{uv}R_v{}^kP_b{}^vRS\&$ $^{uv}R_vS^wR^kC_b$	$^{uv}R_v{}^kC_b{}^{vw}U\&$ $^{uv}R_v{}^vR^kP_bS\&$ $^{uv}R_v{}^kC_b{}^wRS$
	$^{uv}R_v{}^kC_b{}^{vw}U\&$ $^{uv}R_v{}^vR^vR^kP_b{}^{ws}U$ $\&^{uv}R_v{}^kP_bS^{ws}U$	$^{uv}R_v{}^kC_b{}^{vw}U\&$ $^{uv}R_v{}^vR^vR^kC_b{}^sR\&$ $^{uv}R_v{}^vR^kP_bS^vR$	$^{uv}R_v{}^kC_b{}^{vw}U\&$ $^{uv}R_v{}^kP_b{}^vRS\&$ $^{uv}R_vS^kP_b{}^{ws}U$
2	$^{uv}R_v{}^vR^kP_b{}^{vw}U\&$ $^{uv}R_v{}^vR^kP_bS\&$ $^{uv}R_v{}^kC_b{}^wRS$	$^{uv}R_v{}^kP_b{}^vR^{vw}U\&$ $^{uv}R_v{}^kP_b{}^vRS\&$ $^{uv}R_v{}^vR^kP_bS^vR$	$^{uv}R_v{}^kP_b{}^vR^{vw}U\&$ $^{uv}R_v{}^kP_b{}^vRS\&$ $^{uv}R_v{}^{vw}U^kP_bS$
	$^{uv}R_v{}^kP_b{}^vR^{vw}U\&$ $^{uv}R_v{}^kP_b{}^vRS\&$ $^{uv}R_vS^wR^kC_b$	$^{uv}R_v{}^vR^vR^kP_b{}^wR\&$ $^{uv}R_v{}^vR^vR^kP_b{}^{ws}U$ $\&^{uv}R_v{}^{vw}U^kP_bS$	$^{uv}R_v{}^vR^vR^kP_b{}^wR\&$ $^{uv}R_v{}^vR^vR^kP_b{}^{ws}U$ $\&^{uv}R_vS^kP_b{}^{ws}U$
	$^{uv}R_v{}^vR^vR^kP_b{}^wR$ $\&^{uv}R_v{}^kP_b{}^vRS$ $\&^{uv}R_v{}^kP_b{}^{vw}US$	$^{uv}R_v{}^vR^vR^kC_b\&$ $^{uv}R_v{}^vR^vR^kC_b{}^sR\&$ $^{uv}R_v{}^kC_b{}^wRS$	$^{uv}R_v{}^vR^vR^kC_b\&$ $^{uv}R_v{}^vR^vR^kC_b{}^sR$ $\&^{uv}R_v{}^vR^kP_bS^vR$

Table 4 Topology synthesis results of subcategory 3-6-6

Type	Result		
1	${}^{uv}R_v{}^{k}P_b{}^{vw}U$& $2{}^{uv}R_v{}^{k}P_b{}^{vw}US$	${}^{uv}R_v{}^{k}P_b{}^{vw}U$& $2{}^{uv}R_v{}^{k}C_b{}^{w}RS$	${}^{uv}R_v{}^{k}P_b{}^{vw}U$& $2{}^{uv}R_v{}^{v}R^{k}P_bS^{v}R$
	${}^{uv}R_v{}^{k}P_b{}^{vw}U$& $2{}^{uv}R_vS^{k}P_b{}^{ws}U$	${}^{uv}R_v{}^{k}P_b{}^{vw}U$& $2{}^{uv}R_v{}^{vw}U^{k}P_bS$	${}^{uv}R_v{}^{k}P_b{}^{vw}U$& $2{}^{uv}R_vS^{w}R^{k}C_b$
2	${}^{uv}R_v{}^{v}R^{k}P_b{}^{w}R$& $2{}^{uv}R_v{}^{k}P_b{}^{vw}US$	${}^{uv}R_v{}^{v}R^{k}P_b{}^{w}R$& $2{}^{uv}R_v{}^{k}C_b{}^{w}RS$	${}^{uv}R_v{}^{v}R^{k}P_b{}^{w}R$& $2{}^{uv}R_v{}^{v}R^{k}P_bS^{v}R$
	${}^{uv}R_v{}^{v}R^{k}P_b{}^{w}R$& $2{}^{uv}R_vS^{k}P_b{}^{ws}U$	${}^{uv}R_v{}^{v}R^{k}P_b{}^{w}R$& $2{}^{uv}R_v{}^{vw}U^{k}P_bS$	${}^{uv}R_v{}^{v}R^{k}P_b{}^{w}R$& $2{}^{uv}R_vS^{w}R^{k}C_b$
3	${}^{uv}R_v{}^{vw}U^{k}P_b$& $2{}^{uv}R_v{}^{k}P_b{}^{vw}US$	${}^{uv}R_v{}^{vw}U^{k}P_b$& $2{}^{uv}R_v{}^{k}C_b{}^{w}RS$	${}^{uv}R_v{}^{vw}U^{k}P_b$& $2{}^{uv}R_v{}^{v}R^{k}P_bS^{v}R$
	${}^{uv}R_v{}^{vw}U^{k}P_b$& $2{}^{uv}R_vS^{k}P_b{}^{ws}U$	${}^{uv}R_v{}^{vw}U^{k}P_b$& $2{}^{uv}R_v{}^{vw}U^{k}P_bS$	${}^{uv}R_v{}^{vw}U^{k}P_b$& $2{}^{uv}R_vS^{w}R^{k}C_b$

Table 5 Topology evolution results

(${}^{uv}R_v{}^{v}RS$& $2{}^{uv}R_v{}^{v}R^{k}P_bS$)-${}^{k}P_b$	(${}^{uv}R_v{}^{v}R^{v}R^{ws}U$& $2{}^{uv}R_v{}^{v}R^{v}R^{k}P_b{}^{ws}U$)-${}^{k}P_b$	(${}^{uv}R_v{}^{v}R^{v}R^{ks}U$& $2{}^{uv}R_v{}^{v}R^{v}R^{k}C_b{}^{s}R$)-${}^{k}P_b$
(${}^{uv}R_v{}^{v}RS$& $2{}^{uv}R_v{}^{k}P_b{}^{v}RS$)-${}^{k}P_b$	(${}^{uv}R_vS^{w}R$& $2{}^{uv}R_v{}^{v}R^{k}P_bS$)-${}^{k}P_b$	(${}^{uv}R_vS^{w}R$& $2{}^{uv}R_v{}^{k}P_b{}^{v}RS$)-${}^{k}P_b$
(${}^{uv}R_vS$&${}^{uv}R_v{}^{v}R^{k}P_bS$ &${}^{uv}R_v{}^{vw}U^{k}P_bS$)-${}^{k}P_b$	(${}^{uv}R_vS$&${}^{uv}R_v{}^{v}R^{v}R^{k}P_b{}^{ws}U$ &${}^{uv}R_v{}^{k}P_bS^{ws}U$)-${}^{k}P_b$	(${}^{uv}R_vS$&${}^{uv}R_v{}^{v}R^{v}R^{k}C_b{}^{s}R$ &${}^{uv}R_v{}^{v}R^{k}P_bS^{v}R$)-${}^{k}P_b$
(${}^{uv}R_vS$&${}^{uv}R_v{}^{k}P_b{}^{v}RS$ &${}^{uv}R_vS^{k}P_b{}^{ws}U$)-${}^{k}P_b$	(${}^{uv}R_vS$&${}^{uv}R_v{}^{k}P_b{}^{v}RS$ &${}^{uv}R_vS^{w}R^{k}C_b$)-${}^{k}P_b$	(${}^{uv}R_vS$&${}^{uv}R_v{}^{v}R^{k}P_bS$ &${}^{uv}R_v{}^{k}C_b{}^{w}RS$)-${}^{k}P_b$
(${}^{uv}R_v{}^{vw}U$& $2{}^{uv}R_v{}^{k}P_b{}^{vw}US$)-${}^{k}P_b$	(${}^{uv}R_v{}^{vw}U$& $2{}^{uv}R_v{}^{k}C_b{}^{w}RS$)-${}^{k}P_b$	(${}^{uv}R_v{}^{vw}U$& $2{}^{uv}R_v{}^{v}R^{k}P_bS^{v}R$)-${}^{k}P_b$
(${}^{uv}R_v{}^{vw}U$& $2{}^{uv}R_vS^{k}P_b{}^{ws}U$)-${}^{k}P_b$	(${}^{uv}R_v{}^{vw}U$& $2{}^{uv}R_v{}^{vw}U^{k}P_bS$)-${}^{k}P_b$	(${}^{uv}R_v{}^{vw}U$& $2{}^{uv}R_vS^{w}R^{k}C_b$)-${}^{k}P_b$

5.3 Assemble Metamorphic Execution Mechanism

The metamorphic execution mechanism is classified as three subcategories of 3-6-6, 5-5-5, 4-5-6, as shown in Figures 5, 6, 7, where $\dim\{{}^{m}\boldsymbol{S}_{f,L_1}\}-\dim\{{}^{m}\boldsymbol{S}_{f,L_2}\}-\dim\{{}^{m}\boldsymbol{S}_{f,L_3}\}$ denotes the dimension arrangement for three metamorphic limb bonds. Notably, there may exist three approaches to adjusting 3R: (a) Fixed-point spherical motion generated by concurrent rotation joints, it is hard to reconfigure with 2R1T using two types of metamorphic joints assigned; (b) fixed-point or non-concurrent continuous 3R motion generated by one 3R limb and two 6-DOF limbs; (c) general 3R motion with spatially staggered axes by constraining three translations with a general arrangement. It has three variable finite rotation axes and usually produces 3D wide-range parasitic translations. Above all, this study takes (b) and (c) based on the assigned joints.

Subcategory 5-5-5: it utilizes three 5-DOF metamorphic limb bonds and each constrains one translation, leading to three constrained translations of moving platform for adjusting mode. To switch into landing and roving modes with double 2R1T, it should guarantee there exist and only exist two parallel restricted translations—equivalent to one restricted translation and one restricted rotation. So two metamorphic planar-spherical bonds, i.e., $\{{}^{o}\boldsymbol{S}_{f,L_j,32}\}$, must be arranged parallel between two constraint planes. The third limb can be anyone in family 3. Assembly geometric condition for adjusting mode is $\boldsymbol{u}_1=\boldsymbol{u}_2=\boldsymbol{u}_3$. Those for landing and roving modes should be satisfied simultaneously: a) $\boldsymbol{v}_2=\boldsymbol{v}_3$; b) $\boldsymbol{v}_1\neq\boldsymbol{v}_2$, and it's better for $\boldsymbol{v}_1^{\mathrm{T}}\boldsymbol{v}_2=0$. Finally, three types are enumerated in Eq. (23): Type 1 has one common finite rotation and one common finite translation between landing and roving, corresponding to No. 2 in Table 1 so the source phase's dimension is seven. Type 2 or 3 has one common finite rotation between landing and roving, corresponding to No. 1 in Table 1 that the source phase's dimension is eight. In this subcategory, four completely symmetrical topologies can be obtained by Type 2 when all limbs adopt the identical structure; thirty-six partially symmetrical topologies can be obtained requiring two same

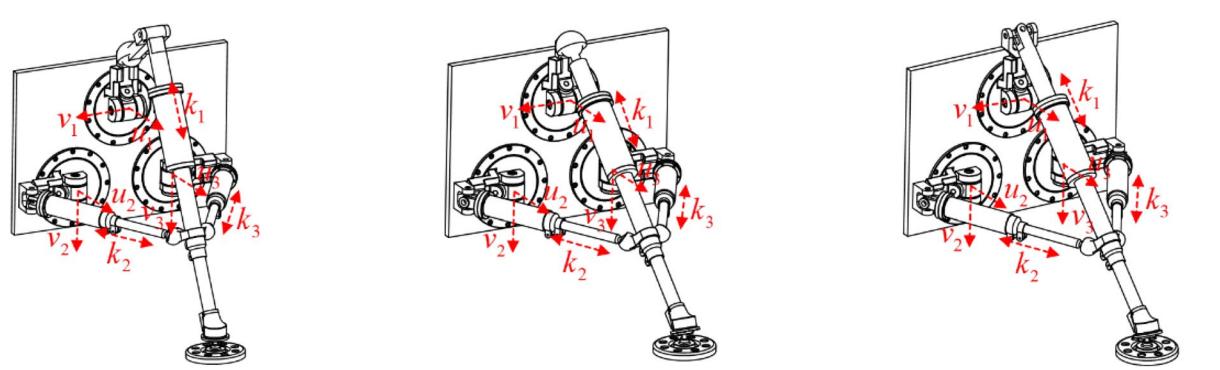

(a) (${}^{uv}R_vS^{w}R$&$2{}^{uv}R_v{}^{v}R^{k}P_bS$)-${}^{k}P_b$ (b) (${}^{uv}R_vS$&${}^{uv}R_v{}^{v}R^{k}P_bS$&${}^{uv}R_v{}^{vw}U^{k}P_bS$)-${}^{k}P_b$ (c) (${}^{uv}R_v{}^{vw}U$&$2{}^{uv}R_v{}^{vw}U^{k}P_bS$)-${}^{k}P_b$

Figure 8 Typical structures based on the topology evolution of three subcategories: **a** (${}^{uv}R_vS^{w}R$&$2{}^{uv}R_v{}^{v}R^{k}P_bS$)-${}^{k}P_b$, **b** (${}^{uv}R_vS$&${}^{uv}R_v{}^{v}R^{k}P_bS$&${}^{uv}R_v{}^{vw}U^{k}P_bS$)-${}^{k}P_b$, **c** (${}^{uv}R_v{}^{vw}U$&$2{}^{uv}R_v{}^{vw}U^{k}P_bS$)-${}^{k}P_b$

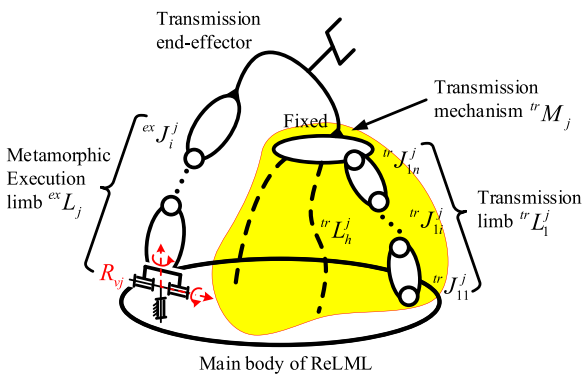

Figure 9 Schematic diagram of the EMPM model

limbs from Type 2, and another limb is casual; there exist a total of ninety-six asymmetrical topologies. For brevity, all symmetrical, twelve partially symmetrical, and five asymmetrical topologies are listed in Table 2. Three typical structures are illustrated in Figure 5.

$$\{{}^o\boldsymbol{S}_{f,Leg}\} = \begin{cases} Type1: \{{}^o\boldsymbol{S}_{f,L_1,31}\} \cap \{{}^o\boldsymbol{S}_{f,L_2,32}\} \cap \{{}^o\boldsymbol{S}_{f,L_3,32}\}, \\ Type2: \{{}^o\boldsymbol{S}_{f,L_1,32}\} \cap \{{}^o\boldsymbol{S}_{f,L_2,32}\} \cap \{{}^o\boldsymbol{S}_{f,L_3,32}\}, \\ Type3: \{{}^o\boldsymbol{S}_{f,L_1,33}\} \cap \{{}^o\boldsymbol{S}_{f,L_2,32}\} \cap \{{}^o\boldsymbol{S}_{f,L_3,32}\}. \end{cases} \tag{23}$$

Subcategory 4-5-6: It employs one 4-DOF, one 5-DOF, and a full-mobility metamorphic limb bonds. (1) Type 1: in each mode, the 4-DOF bond always constrains two translations, the 5-DOF bond always constrains one translation (unparallel to the restricted translation plane in adjusting mode, and parallel to the constrained translation plane in landing and roving modes). So the 4-DOF bond must be $\{{}^o\boldsymbol{S}_{f,L_1,21}\}$, the 5-DOF one must be $\{{}^o\boldsymbol{S}_{f,L_2,32}\}$, they both contain the planar-spherical bond. Assembly geometric condition for adjusting is $\boldsymbol{u}_1 = \boldsymbol{u}_2 = \boldsymbol{u}_3$, for landing and roving is $\boldsymbol{v}_1 = \boldsymbol{v}_2$. This type has one common rotation between adjusting and landing/roving, two common rotations between landing and roving, and one common rotation among three modes. It corresponds to No. 5 in Table 1 with the source phase dimension of six; (2) Type 2: the 4-DOF bond in adjusting mode constrains two translations, and in landing and roving modes constrains one translation and one rotation. The 5-DOF bond always constrains a translation (independent with two constrained translations in adjusting mode, and unparallel to the constrained translation in landing and roving modes). Hence, the 4-DOF bond must be $\{{}^o\boldsymbol{S}_{f,L_1,22}\}$, the 5-DOF bond can be anyone in family 3. Assembly geometric condition for adjusting is $\boldsymbol{u}_1 = \boldsymbol{u}_2 = \boldsymbol{u}_3$, for landing and roving modes is $\boldsymbol{v}_1 \neq \boldsymbol{v}_2$ ($\boldsymbol{v}_1^{\mathrm{T}}\boldsymbol{v}_2 = 0$ is better). This type has one common rotation between adjusting and landing/roving, three common motions between landing and roving, one common rotation among three modes. It corresponds to No. 6 in Table 1 with the source phase dimension being five. The above types are enumerated in Eq. (24). For brevity, nine typical structures in each type are listed in Table 3. Three of them are shown in Figure 6.

$$\{{}^o\boldsymbol{S}_{f,Leg}\} = \begin{cases} Type1: \{{}^o\boldsymbol{S}_{f,L_1,21}\} \cap \{{}^o\boldsymbol{S}_{f,L_2,32}\} \cap \{{}^o\boldsymbol{S}_{f,L_3,4N_t}\}, \\ Type2: \{{}^o\boldsymbol{S}_{f,L_1,22}\} \cap \{{}^o\boldsymbol{S}_{f,L_2,3N_t}\} \cap \{{}^o\boldsymbol{S}_{f,L_3,4N_t}\}. \end{cases} \tag{24}$$

Subcategory 3-6-6: It has the simplest assembly without any special geometric condition. One limb is from family 1 offering three motions and three constraints in each mode; the other two limbs from family 4 are always full-mobility. This subcategory always has two common finite rotations between/among modes. So it corresponds to No. 15 in Table 1 with the source phase having five dimensions. Based on the bond variations of limb 1, three types are enumerated in Eq. (25), and some practical results are listed in Table 4 and illustrated in Figure 7.

$$\{{}^o\boldsymbol{S}_{f,Leg}\} = \begin{cases} Type1: \{{}^o\boldsymbol{S}_{f,L_1,11}\} \cap \{{}^o\boldsymbol{S}_{f,L_2,4N_t}\} \cap \{{}^o\boldsymbol{S}_{f,L_3,4N_t}\}, \\ Type2: \{{}^o\boldsymbol{S}_{f,L_1,12}\} \cap \{{}^o\boldsymbol{S}_{f,L_2,4N_t}\} \cap \{{}^o\boldsymbol{S}_{f,L_3,4N_t}\}, \\ Type3: \{{}^o\boldsymbol{S}_{f,L_1,13}\} \cap \{{}^o\boldsymbol{S}_{f,L_2,4N_t}\} \cap \{{}^o\boldsymbol{S}_{f,L_3,4N_t}\}. \end{cases} \tag{25}$$

Topology evolution: The above subcategories build metamorphic parallel topologies, of which, the landing mode adopts the inverse-tripod type truss (validated in Phoenix, Tianwen, etc. stationary landers). Here, we aim to derive novel metamorphic hybrid ones that share the identical adjusting and roving topologies, but

Table 6 Number synthesis for the metamorphic transmission

No.	$\{^aS\}$	$\{^rS\}$	$\bigcap_{m=a,r}\{^mS\}$	$\{^oS\}$	N_p	N_a
1	1	1	0	2	1	1
2	2	2	1	3	1	2
3	3	3	2	4	1	3
4	4	4	3	5	1	4
5	5	5	4	6	1	5
6	6	6	5	7	1	6

a different landing one adopting the cantilever-type truss (like Apollo, Chang'E landers, etc.). The evolution only affects the passive metamorphosis for a more credible topology and better input-output decoupling property. Six cases of each subcategory are listed in Table 5, representatives are depicted in Figure 8.

6 Topology Synthesis of Metamorphic Transmission Mechanism for Adjusting, Landing, Roving

6.1 Determine Multi-Mode Output Motion by EMPM

The transmission mechanism is connected with the execution limb to drive adjusting and roving motions, and protect the fragile actuation from large touchdown impact. The equivalent metamorphic parallel mechanism (EMPM) model is built for topological correlation, illustrated in Figure 9: transmission mechanism ${}^{tr}M_j$ corresponds to execution limb ${}^{ex}L_j$, which is the only passive limb to be actuated with multiple outputs. Furthermore, ${}^{ex}J_i^j$ is the ith joint of ${}^{ex}L_j$, and ${}^{tr}L_h^j$ is the hth transmission limb of ${}^{tr}M_j$.

Utilizing the De Morgan's law, the dimension of source metamorphic transmission mechanism can be obtained by

$$\begin{aligned}&\dim\left\{{}^{o}\boldsymbol{S}_{f,Trans}\right\}=\dim\left(\bigcup_{\mathrm{m}=a,r}\left\{{}^{\mathrm{m}}\boldsymbol{S}_{f,Trans}\right\}\right)\\&=\dim\left\{{}^{a}\boldsymbol{S}_{f,Trans}\right\}+\dim\left\{{}^{r}\boldsymbol{S}_{f,Trans}\right\}-\dim\left(\bigcap_{\mathrm{m}=a,r}\left\{{}^{\mathrm{m}}\boldsymbol{S}_{f,Trans}\right\}\right).\end{aligned}\tag{26}$$

Moreover, the effective EMPM model without redundant actuation and overconstraint should satisfy the following topology construction conditions:

$$\begin{aligned}&N=N_a+N_p,\\&F_D=\sum_{j=1}^{N}q_j,\ \dim\left\{{}^{\mathrm{m}}\boldsymbol{S}_{f,Trans}\right\}\le F_D\le\dim\left\{{}^{o}\boldsymbol{S}_{f,Trans}\right\},\end{aligned}\tag{27}$$

where N is the sum of active and passive limb numbers N_a and N_p, and $N_p=1$ in this study. F_D is the DOF of the source metamorphic transmission mechanism, q_j is the actuation number of the jth transmission limb. There always exists $\dim\left\{{}^{o}\boldsymbol{S}_{f,Trans}\right\}-\dim\left\{{}^{\mathrm{m}}\boldsymbol{S}_{f,Trans}\right\}=1$. $F_D=\dim\left\{{}^{\mathrm{m}}\boldsymbol{S}_{f,Trans}\right\}$ indicates all modes are actuated by the same motors.

Bringing Eqs. (26)–(27) into account, Table 6 obtains the number synthesis results: No.1 is the most feasible with single-motor-input and multi-mode-output property. Actually, given that big mobility of ${}^{ex}L_j$ will lead to more joints, limbs, motors in ${}^{tr}M_j$. Hence, the transmission mechanism here is designed to connect the first link of execution limb. Finally, it should guarantee the multiple output motions that the rotation around axis u for adjusting, rigid connection for landing, rotation around axis v for roving, formulated as:

$$\left\{{}^{\mathrm{m}}\boldsymbol{S}_{f,Trans}\right\}=\left\{{}^{\mathrm{m}}\boldsymbol{S}_{f,R_v}\right\}.\tag{28}$$

6.2 Determine Kinematic Bond of Transmission Limb

The finite motion of the source metamorphic transmission mechanism is the united set of adjusting and roving motions, given as:

$$\begin{aligned}&\left\{{}^{o}\boldsymbol{S}_{f,Trans}\right\}=\left\{{}^{a}\boldsymbol{S}_{f,Trans}\right\}\cup\left\{{}^{r}\boldsymbol{S}_{f,Trans}\right\},\\&\Rightarrow{}^{o}\boldsymbol{S}_{f,Trans}=2\tan\frac{\theta_v}{2}\begin{pmatrix}\boldsymbol{v}\\\boldsymbol{r}\times\boldsymbol{v}\end{pmatrix}\Delta 2\tan\frac{\theta_u}{2}\begin{pmatrix}\boldsymbol{u}\\\boldsymbol{r}\times\boldsymbol{u}\end{pmatrix}.\end{aligned}\tag{29}$$

Table 7 Topology synthesis results of the metamorphic transmission mechanism

Subcategory	Result			
$\dim\{{}^{o}\boldsymbol{S}_{f,L_2}\}=5$	${}^{u}\mathrm{P}^{u}\mathrm{R}^{u}\mathrm{R}^{v}\mathrm{R}\&{}^{uv}\mathrm{R}_{v}$	${}^{u}\mathrm{C}^{u}\mathrm{R}^{u}\mathrm{R}^{v}\mathrm{R}\&{}^{uv}\mathrm{R}_{v}$	${}^{u}\mathrm{P}^{u}\mathrm{R}^{u}\mathrm{R}^{uv}\mathrm{U}\&{}^{uv}\mathrm{R}_{v}$	${}^{u}\mathrm{C}^{u}\mathrm{R}^{uv}\mathrm{U}\&{}^{uv}\mathrm{R}_{v}$
	${}^{v}\mathrm{P}^{v}\mathrm{R}^{v}\mathrm{R}^{v}\mathrm{R}^{u}\mathrm{R}\&{}^{uv}\mathrm{R}_{v}$	${}^{v}\mathrm{C}^{v}\mathrm{R}^{v}\mathrm{R}^{u}\mathrm{R}\&{}^{uv}\mathrm{R}_{v}$	${}^{v}\mathrm{P}^{v}\mathrm{R}^{v}\mathrm{R}^{vu}\mathrm{U}\&{}^{uv}\mathrm{R}_{v}$	${}^{v}\mathrm{C}^{v}\mathrm{R}^{vu}\mathrm{U}\&{}^{uv}\mathrm{R}_{v}$
	${}^{v}\mathrm{R}^{v}\mathrm{R}^{v}\mathrm{R}^{u}\mathrm{R}^{u}\mathrm{R}\&{}^{uv}\mathrm{R}_{v}$	${}^{v}\mathrm{R}^{v}\mathrm{R}^{vu}\mathrm{U}^{u}\mathrm{R}\&{}^{uv}\mathrm{R}_{v}$	${}^{u}\mathrm{R}^{u}\mathrm{R}^{u}\mathrm{R}^{v}\mathrm{R}^{v}\mathrm{R}\&{}^{uv}\mathrm{R}_{v}$	${}^{u}\mathrm{R}^{u}\mathrm{R}^{uv}\mathrm{U}^{v}\mathrm{R}\&{}^{uv}\mathrm{R}_{v}$
	${}^{u}\mathrm{R}^{u}\mathrm{R}^{v}\mathrm{R}^{v}\mathrm{R}^{v}\mathrm{R}\&{}^{uv}\mathrm{R}_{v}$	${}^{u}\mathrm{R}^{uv}\mathrm{U}^{v}\mathrm{R}^{v}\mathrm{R}\&{}^{uv}\mathrm{R}_{v}$	${}^{v}\mathrm{R}^{v}\mathrm{R}^{u}\mathrm{R}^{u}\mathrm{R}^{u}\mathrm{R}\&{}^{uv}\mathrm{R}_{v}$	${}^{v}\mathrm{R}^{vu}\mathrm{U}^{u}\mathrm{R}^{u}\mathrm{R}\&{}^{uv}\mathrm{R}_{v}$
$\dim\{{}^{o}\boldsymbol{S}_{f,L_2}\}=6$	${}^{u}\mathrm{P}^{u}\mathrm{R}^{u}\mathrm{RS}\&{}^{uv}\mathrm{R}_{v}$	${}^{u}\mathrm{C}^{u}\mathrm{RS}\&{}^{uv}\mathrm{R}_{v}$	${}^{v}\mathrm{P}^{v}\mathrm{R}^{v}\mathrm{RS}\&{}^{uv}\mathrm{R}_{v}$	${}^{v}\mathrm{C}^{v}\mathrm{RS}\&{}^{uv}\mathrm{R}_{v}$
	${}^{v}\mathrm{R}^{v}\mathrm{R}^{v}\mathrm{R}^{u}\mathrm{R}^{uw}\mathrm{U}\&{}^{uv}\mathrm{R}_{v}$	${}^{v}\mathrm{R}^{v}\mathrm{R}^{vu}\mathrm{U}^{uw}\mathrm{U}\&{}^{uv}\mathrm{R}_{v}$	${}^{u}\mathrm{R}^{u}\mathrm{R}^{u}\mathrm{R}^{v}\mathrm{R}^{vw}\mathrm{U}\&{}^{uv}\mathrm{R}_{v}$	${}^{u}\mathrm{R}^{u}\mathrm{R}^{uv}\mathrm{U}^{vw}\mathrm{U}\&{}^{uv}\mathrm{R}_{v}$
	${}^{u}\mathrm{R}^{u}\mathrm{R}^{v}\mathrm{R}^{v}\mathrm{R}^{vw}\mathrm{U}\&{}^{uv}\mathrm{R}_{v}$	${}^{u}\mathrm{R}^{uv}\mathrm{U}^{v}\mathrm{R}^{vw}\mathrm{U}\&{}^{uv}\mathrm{R}_{v}$	${}^{v}\mathrm{R}^{v}\mathrm{R}^{u}\mathrm{R}^{u}\mathrm{R}^{uw}\mathrm{U}\&{}^{uv}\mathrm{R}_{v}$	${}^{v}\mathrm{R}^{vu}\mathrm{U}^{u}\mathrm{R}^{uw}\mathrm{U}\&{}^{uv}\mathrm{R}_{v}$
	${}^{v}\mathrm{R}^{vw}\mathrm{US}\&{}^{uv}\mathrm{R}_{v}$	${}^{v}\mathrm{RSU}\&{}^{uv}\mathrm{R}_{v}$	${}^{u}\mathrm{R}^{uw}\mathrm{US}\&{}^{uv}\mathrm{R}_{v}$	${}^{u}\mathrm{RSU}\&{}^{uv}\mathrm{R}_{v}$
	${}^{v}\mathrm{P}^{uw}\mathrm{US}\&{}^{uv}\mathrm{R}_{v}$	${}^{v}\mathrm{PSU}\&{}^{uv}\mathrm{R}_{v}$	${}^{u}\mathrm{P}^{vw}\mathrm{US}\&{}^{uv}\mathrm{R}_{v}$	${}^{u}\mathrm{PSU}\&{}^{uv}\mathrm{R}_{v}$
	${}^{v}\mathrm{C}^{vw}\mathrm{U}^{ws}\mathrm{U}\&{}^{uv}\mathrm{R}_{v}$	${}^{v}\mathrm{C}^{v}\mathrm{RS}\&{}^{uv}\mathrm{R}_{v}$	${}^{v}\mathrm{C}^{u}\mathrm{RS}\&{}^{uv}\mathrm{R}_{v}$	${}^{v}\mathrm{CSR}\&{}^{uv}\mathrm{R}_{v}$
	${}^{u}\mathrm{C}^{uw}\mathrm{U}^{ws}\mathrm{U}\&{}^{uv}\mathrm{R}_{v}$	${}^{u}\mathrm{C}^{u}\mathrm{RS}\&{}^{uv}\mathrm{R}_{v}$	${}^{u}\mathrm{C}^{v}\mathrm{RS}\&{}^{uv}\mathrm{R}_{v}$	${}^{u}\mathrm{CSR}\&{}^{uv}\mathrm{R}_{v}$
	${}^{v}\mathrm{RSS}\&{}^{uv}\mathrm{R}_{v}$*	${}^{u}\mathrm{RSS}\&{}^{uv}\mathrm{R}_{v}$*	${}^{v}\mathrm{PSS}\&{}^{uv}\mathrm{R}_{v}$*	${}^{u}\mathrm{PSS}\&{}^{uv}\mathrm{R}_{v}$*

Note: The results marked with * have an idle DOF generated by the SS link

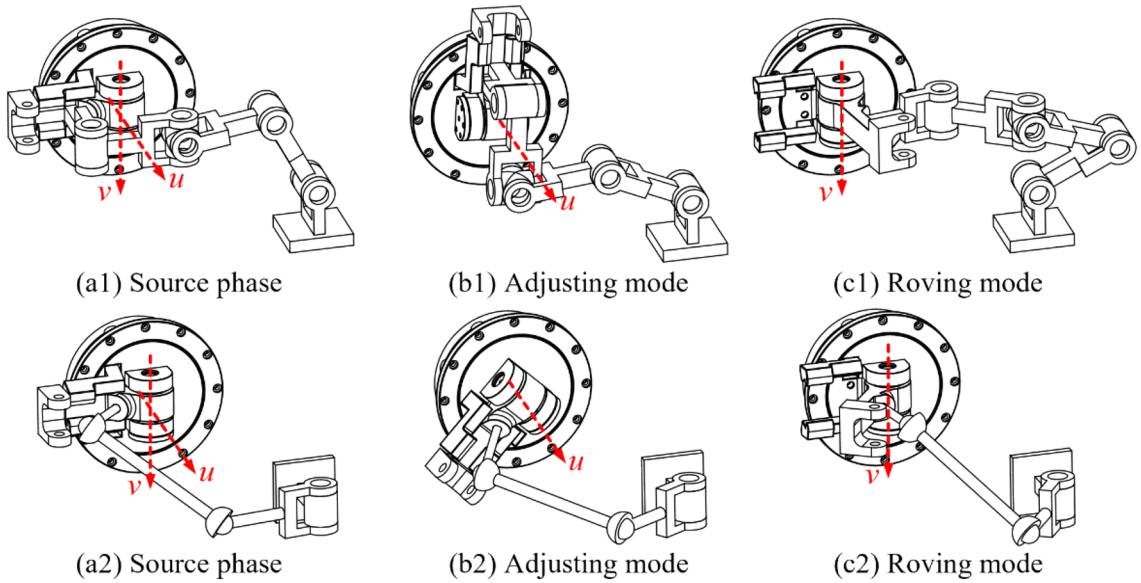

Figure 10 Typical structures of metamorphic transmission mechanism: **a1**–**c1** are ${}^{u}\mathrm{R}^{u}\mathrm{R}^{uv}\mathrm{U}^{v}\mathrm{R}\&{}^{uv}\mathrm{Rv}$, **a2**–**c2** are ${}^{v}\mathrm{RSS}\&{}^{uv}\mathrm{Rv}$

According to the EMEM model of metamorphic transmission mechanism, its finite output motion is the intersection of ${}^{\mathrm{m}}\mathrm{R}_{\mathrm{v}}$ and transmission limb, expressed as:

$$\begin{aligned}&\left\{{}^{\mathrm{m}}\boldsymbol{S}_{f,Trans}\right\}=\left\{{}^{\mathrm{m}}\boldsymbol{S}_{f,R_v}\right\}=\left\{{}^{\mathrm{m}}\boldsymbol{S}_{f,R_v}\right\}\cap\left\{{}^{\mathrm{m}}\boldsymbol{S}_{f,L_t}\right\},\\&\Rightarrow\left\{{}^{o}\boldsymbol{S}_{f,L_t}\right\}\supseteq\left\{{}^{o}\boldsymbol{S}_{f,Trans}\right\}.\end{aligned}\tag{30}$$

There are two families of source metamorphic bonds $\left\{{}^{o}\boldsymbol{S}_{f,L_t}\right\}$, and each contains two orthogonal rotation factors. The mechanical generators are only allowed with at most one prismatic joint besides actuation for practice.

(1) Subcategory 1: $\dim\{{}^{o}\boldsymbol{S}_{f,L_t}\}=5$. According to the intersection condition to generate rotation, there must be two finite translations lying in the normal plane of rotation axis. Hence, we add two translation factors orthogonal to each rotation factor respectively in Eq. (29), and finally obtain the standard type with five independent factors:

$$\begin{aligned}\left\{{}^{o}\boldsymbol{S}_{f,L_t,1}\right\}&=\left\{t_v\begin{pmatrix}\boldsymbol{0}\\\boldsymbol{v}\end{pmatrix}\Delta t_n\begin{pmatrix}\boldsymbol{0}\\\boldsymbol{n}\end{pmatrix}\Delta 2\tan\frac{\theta_u}{2}\begin{pmatrix}\boldsymbol{u}\\\boldsymbol{r}\times\boldsymbol{u}\end{pmatrix}\right\}\\&\cup\left\{t_u\begin{pmatrix}\boldsymbol{0}\\\boldsymbol{u}\end{pmatrix}\Delta t_n\begin{pmatrix}\boldsymbol{0}\\\boldsymbol{n}\end{pmatrix}\Delta 2\tan\frac{\theta_v}{2}\begin{pmatrix}\boldsymbol{v}\\\boldsymbol{r}\times\boldsymbol{v}\end{pmatrix}\right\}\\&\Rightarrow{}^{o}\boldsymbol{S}_{f,L_t,1}=2\tan\frac{\theta_v}{2}\begin{pmatrix}\boldsymbol{v}\\\boldsymbol{r}\times\boldsymbol{v}\end{pmatrix}\Delta 2\tan\frac{\theta_u}{2}\begin{pmatrix}\boldsymbol{u}\\\boldsymbol{r}\times\boldsymbol{u}\end{pmatrix}\\&\Delta\left(t_n\begin{pmatrix}\boldsymbol{0}\\\boldsymbol{n}\end{pmatrix}+t_v\begin{pmatrix}\boldsymbol{0}\\\exp(\theta_u\tilde{\boldsymbol{u}})\boldsymbol{v}\end{pmatrix}+t_u\begin{pmatrix}\boldsymbol{0}\\\exp(\theta_u\tilde{\boldsymbol{u}})\exp(\theta_v\tilde{\boldsymbol{v}})\boldsymbol{u}\end{pmatrix}\right),\end{aligned}$$

which can be rewritten as:

$$\begin{aligned}{}^{o}\boldsymbol{S}_{f,L_t,1}&=2\tan\frac{\theta_v}{2}\begin{pmatrix}\boldsymbol{v}\\\boldsymbol{r}_2\times\boldsymbol{v}\end{pmatrix}\Delta 2\tan\frac{\theta_u}{2}\begin{pmatrix}\boldsymbol{u}\\\boldsymbol{r}_1\times\boldsymbol{u}\end{pmatrix}\\&\Delta t_n\begin{pmatrix}\boldsymbol{0}\\\boldsymbol{n}\end{pmatrix}\Delta t_v\begin{pmatrix}\boldsymbol{0}\\\boldsymbol{v}\end{pmatrix}\Delta t_u\begin{pmatrix}\boldsymbol{0}\\\boldsymbol{u}\end{pmatrix}.\end{aligned}\tag{31}$$

(2) Subcategory 2: $\dim\{{}^{o}\boldsymbol{S}_{f,L_t}\}=6$. Adding a rotation factor to the left side of Eq. (31), expressed as:

$$\begin{aligned}{}^{o}\boldsymbol{S}_{f,L_t,2}&=2\tan\frac{\theta_3}{2}\begin{pmatrix}\boldsymbol{n}\\\boldsymbol{r}_3\times\boldsymbol{n}\end{pmatrix}\Delta 2\tan\frac{\theta_v}{2}\begin{pmatrix}\boldsymbol{v}\\\boldsymbol{r}_2\times\boldsymbol{v}\end{pmatrix}\\&\Delta 2\tan\frac{\theta_u}{2}\begin{pmatrix}\boldsymbol{u}\\\boldsymbol{r}_1\times\boldsymbol{u}\end{pmatrix}\Delta t_n\begin{pmatrix}\boldsymbol{0}\\\boldsymbol{n}\end{pmatrix}\Delta t_v\begin{pmatrix}\boldsymbol{0}\\\boldsymbol{v}\end{pmatrix}\Delta t_u\begin{pmatrix}\boldsymbol{0}\\\boldsymbol{u}\end{pmatrix}.\end{aligned}\tag{32}$$

6.3 Design Mechanical Generator and Assemble

The standard structures of the above two subcategories are ${}^{u}\mathrm{P}^{v}\mathrm{P}^{n}\mathrm{P}^{u}\mathrm{R}^{v}\mathrm{R}$ and ${}^{u}\mathrm{P}^{v}\mathrm{P}^{n}\mathrm{P}^{u}\mathrm{R}^{v}\mathrm{R}^{n}\mathrm{R}$. Considering the practical demand upon transmission limb, it is only allowed to possess one prismatic joint as actuation. So derivative structures should be targetedly obtained by joint type and location substitutions based on screw triangle product. Given transmission limb has a single-open chain topology, we directly give the structures of source metamorphic transmission mechanism in Table 7. Assembly geometric conditions for subcategory 1: There should be a planar motion (two translations, one rotation) orthogonal to axis u in adjusting mode, and the other planar motion orthogonal to axis v in roving mode. No specific condition is required for subcategory 2. Two typical structures of metamorphic transmission mechanism are illustrated in Figure 10.

For conciseness, the first subcategory is taken for instance to demonstrate the derivation process, because the second subcategory with 6 DOFs is easier to obtain. The kinematic bond in Eq. (31) is equivalent to the first row of Eq. (33), of which, the second factor is rotation around axis u, the third and fourth factors indicate circular translations with radii of $\|\boldsymbol{r}_3-\boldsymbol{r}_2\|$ and $\|\boldsymbol{r}_2-\boldsymbol{r}_1\|$ respectively around u. When $\|\boldsymbol{r}_3-\boldsymbol{r}_2\|\to\infty$ and $\|\boldsymbol{r}_2-\boldsymbol{r}_1\|\to\infty$, the third to sixth factors operated by screw triangle product are equivalent to three translations in Eq. (31). Moreover, the first row of Eq. (33) is derived from the second row, resulting in the structure of ${}^{u}\mathrm{P}^{u}\mathrm{R}^{u}\mathrm{R}^{u}\mathrm{R}^{v}\mathrm{R}$ in subcategory 1. Further, the third row derives the derivative structure of ${}^{u}\mathrm{C}^{u}\mathrm{R}^{uv}\mathrm{U}$ by the joint type substitution when letting $\boldsymbol{r}_3=\boldsymbol{r}_4$, and one can still derive ${}^{u}\mathrm{C}^{u}\mathrm{R}^{u}\mathrm{R}^{v}\mathrm{R}$ and ${}^{u}\mathrm{P}^{u}\mathrm{R}^{u}\mathrm{R}^{uv}\mathrm{U}$ from this equation:

$$
\begin{aligned}
&{}^{o}\boldsymbol{S}_{f,L_t,1}\\
&\Leftrightarrow 2\tan\frac{\theta_4}{2}\begin{pmatrix}\boldsymbol{v}\\ \boldsymbol{r}_4\times\boldsymbol{v}\end{pmatrix}\Delta 2\tan\frac{\sum_{i=1}^{3}\theta_i}{2}\begin{pmatrix}\boldsymbol{u}\\ \boldsymbol{r}_3\times\boldsymbol{u}\end{pmatrix}\Delta\begin{pmatrix}\boldsymbol{0}\\ \left(\exp(\sum_{i=1}^{2}\theta_i\tilde{\boldsymbol{u}})-\boldsymbol{I}_3\right)(\boldsymbol{r}_3-\boldsymbol{r}_2)\end{pmatrix}\\
&\quad\Delta\begin{pmatrix}\boldsymbol{0}\\ (\exp(\theta_1\tilde{\boldsymbol{u}})-\boldsymbol{I}_3)(\boldsymbol{r}_2-\boldsymbol{r}_1)\end{pmatrix}\Delta t_u\begin{pmatrix}\boldsymbol{0}\\ \boldsymbol{u}\end{pmatrix}\\
&=2\tan\frac{\theta_4}{2}\begin{pmatrix}\boldsymbol{v}\\ \boldsymbol{r}_4\times\boldsymbol{v}\end{pmatrix}\Delta 2\tan\frac{\theta_3}{2}\begin{pmatrix}\boldsymbol{u}\\ \boldsymbol{r}_3\times\boldsymbol{u}\end{pmatrix}\Delta 2\tan\frac{\theta_2}{2}\begin{pmatrix}\boldsymbol{u}\\ \boldsymbol{r}_2\times\boldsymbol{u}\end{pmatrix}\\
&\quad\Delta 2\tan\frac{\theta_1}{2}\begin{pmatrix}\boldsymbol{u}\\ \boldsymbol{r}_1\times\boldsymbol{u}\end{pmatrix}\Delta t_u\begin{pmatrix}\boldsymbol{0}\\ \boldsymbol{u}\end{pmatrix}\\
&=\left(2\tan\frac{\theta_4}{2}\begin{pmatrix}\boldsymbol{v}\\ \boldsymbol{r}_3\times\boldsymbol{v}\end{pmatrix}\Delta 2\tan\frac{\theta_3}{2}\begin{pmatrix}\boldsymbol{u}\\ \boldsymbol{r}_3\times\boldsymbol{u}\end{pmatrix}\right)_U\Delta 2\tan\frac{\theta_2}{2}\begin{pmatrix}\boldsymbol{u}\\ \boldsymbol{r}_2\times\boldsymbol{u}\end{pmatrix}\\
&\quad\Delta\left(2\tan\frac{\theta_1}{2}\begin{pmatrix}\boldsymbol{u}\\ \boldsymbol{r}_1\times\boldsymbol{u}\end{pmatrix}+t_u\begin{pmatrix}\boldsymbol{0}\\ \boldsymbol{u}\end{pmatrix}\right)_C.
\end{aligned}
\tag{33}
$$

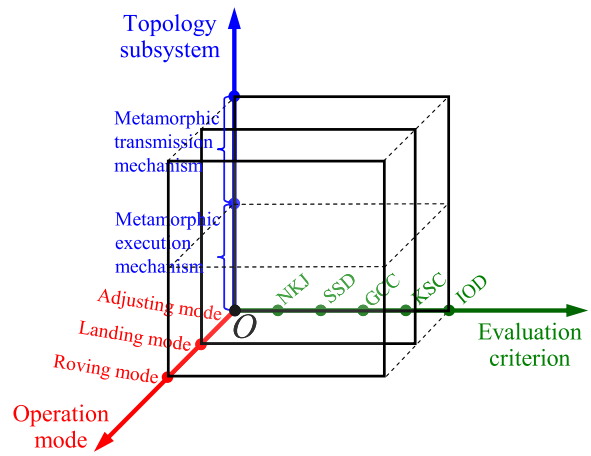

Figure 11 3D optimal selection matrix method

7 Multi-Mode and Multi-Criterion Optimal Selection and Prototype Simulation of ReLML

The topological evaluation criteria for the metamorphic topology system of ReLML are presented.

Criterion 1: Number of kinematic joint (NKJ). It is the sum of all kinematic joints of a mechanism to represent the topological simplicity. Obviously, it should be as small as possible. For this study, the NKJs of three modes are equal and three smaller than that of the source phase.

Criterion 2: Structural symmetry degree (SSD). It describes the interchangeability of subchain for a mechanism to facilitate manufacture, maintenance, etc.

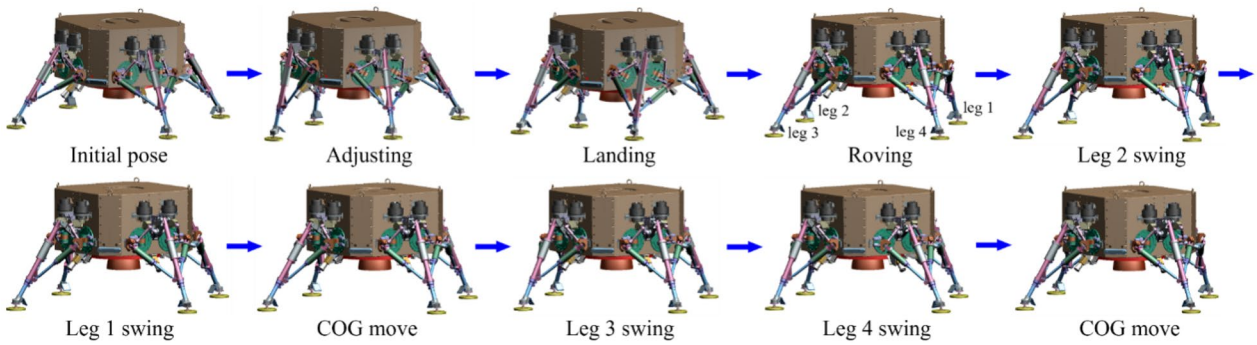

Figure 12 Simulation of ReLML to explore the hostile extraterrestrial landform

Specifically, for a parallel topology, SSD refers to the ratio between the maximum sum of identical subchains' DOFs among limbs and the sum of all limbs' DOFs; for a serial topology, SSD refers to the ratio between the maximum sum of identical joints' DOFs and the serial topology's DOFs. Obviously, a completely symmetric topology produces the most ideal circumstance and $SSD=1$.

$$SSD = \max\left(n_s \cdot f_{sn}\right) / \sum_{j=1}^{N} f_j, \tag{34}$$

where n_s and f_{sn} are the number and DOF of identical subchains between limbs respectively, f_j is the jth limb's DOF.

Criterion 3: Geometric constraint complexity (GCC). It reflects the difficulty to assemble limbs and platforms into a mechanism, and to reliably keep motion characteristics. GCC is calculated by the geometric constraints in the limb, and among limbs to connect platform. For instance, 1-dimensional constraint contains the parallel or orthogonal condition of two rotations/translations; 2-dimension constraints happen in the planar motion of a RRR subchain, due to two independent parallel conditions among axes; 3-dimension constraints occur when three rotations intersect with the same point, etc. The topology with a lower GCC is better for assembly and payload.

$$GCC = \sum_{j=1}^{N}\sum_{k=1}^{K} k \cdot C_k^{in} + \sum_{k=1}^{K} k \cdot C_k^{am}, \tag{35}$$

where k is the dimension of some specific geometric constraint ($k=1-6$), C_k^{in} is the number of k-dimension geometric constraint to assemble the limb, and C_k^{am} is that among limbs to be connected with platforms.

Criterion 4: Kinematic solution complexity (KSC), also knowns as coupling degree [39]. It reveals the difficulty degree of position modeling and solution, and is only affected by topology. KSC is related to the smallest dimension of closed-loop position equations when combining and solving, with the guiding significance for optimal selection, kinematic and dynamic analyses. Definitely, KSC is required to be as smaller as possible.

Criterion 5: Input-output decoupling (IOD), also called I-O decoupling [39, 44]. In this study, it measures the number of independent output motions only controlled by one specific actuated joint. The metamorphic subsystem of ReLML with more degrees of IOD will enhance the capability of landing buffer, and also facilitate motion planning and control when adjusting and roving modes.

Thus, a 3D optimal selection matrix method is proposed, as shown in Figure 11, to illustrate relationships among operation modes, topology subsystems, and evaluation criteria. Table 8 is its 2D form to systematically present the quantitative correlations. To evaluate each criterion, the values of three modes and the corresponding weighted averages (WAs) are calculated, here they are 1/3. In the WA column, a symbol after WA is attached to assign the practicability judged by designer, ● means satisfaction, ◑ means partial satisfaction, ○ means not satisfaction. Finally, the practicability values in the last column can be obtained for optimal selection. From Table 8, we can conclude: (1) Topology evolution of metamorphic execution mechanism just influences the values of SSD and IOD in landing mode, and others are not affected; (2) subcategory 5-5-5 and its evolution behave the best practicability as execution; (3) subcategory 2 presents the best practicability as transmission. Finally, No. 17 and No. 21 are selected to combine into the complete metamorphic topology system of ReLML.

Finally, the prototype construction integrating active and passive metamorphoses are identified, see Figure 1. For engineering practice, we design ${}^{m}R_v$ in primary limb with just rigid and v-axis rotation phases. So the metamorphic execution is $({}^{v}R_v{}^{vw}U\&2^{uv}R_v{}^{vw}U^{k}P_bS)\text{-}{}^{k}P_b$. Compared with No. 17, it has identical landing and roving

Table 8 Multi-mode & multi-criterion optimal selection for the metamorphic topology system of ReLML

No.		Metamorphic topology subsystem	NKJ	SSD				GCC				KSC				IOD				Practicability
			a/l/r	*a*	*l*	*r*	WA	*a*	*l*	*r*	WA	*a*	*l*	*r*	WA	*a*	*l*	*r*	WA	
1	Execution	$3^{uv}R_v{}^vR^kP_bS$	9●	1	1	1	1●	2	2	5	3◑	1	1	1	1◑	0	0	0	0◑	●●●◑
2		$3^{uv}R_v{}^vR^vR^kP_b{}^{ws}U$	12○	1	1	1	1●	5	5	8	6○	2	2	2	2○	0	0	0	0◑	●◑
3		$^{uv}R_vS^wR^kP_b\&2^{uv}R_v{}^vR^kP_bS$	9●	0.67	0.67	0.67	0.67◑	2	2	4	2.67◑	1	1	1	1◑	0	0	0	0◑	●●●
4		$^{uv}R_v{}^kP_bS\&^{uv}R_v{}^vR^kP_bS\&^{uv}R_v{}^{vw}U^kP_bS$	8●	0.6	0.8	0.6	0.67◑	2	1	2	1.67●	0	0	0	0●	0	0	0	0◑	●●●●
5		$^{uv}R_v{}^vR^kP_b{}^{vw}U\&^{uv}R_v{}^vR^kP_bS$ $\&^{uv}R_vS^kP_b{}^{ws}U$	9●	0.27	0.4	0.27	0.31○	3	2	4	3◑	0	0	0	0●	0	0	0	0◑	●●●
6		$^{uv}R_v{}^vR^vR^kP_b{}^wR\&^{uv}R_v{}^vR^vR^kP_b{}^{ws}U$ $\&^{uv}R_v{}^{vw}U^kP_bS$	11◑	0.4	0.4	0.4	0.4○	4	4	5	4.33◑	0	0	0	0●	0	0	0	0◑	●●◑
7		$^{uv}R_v{}^kP_b{}^{vw}U\&2^{uv}R_v{}^{vw}U^kP_bS$	8●	0.8	0.8	0.8	0.8●	0	0	1	0.33●	0	0	0	0●	0	0	0	0◑	●●●●◑
8		$^{uv}R_v{}^vR^kP_b{}^wR\&2^{uv}R_vS^kP_b{}^{ws}U$	9●	0.8	0.8	0.8	0.8●	0	0	1	0.33●	0	0	0	0●	0	0	0	0◑	●●●●◑
9		$^{uv}R_v{}^{vw}U^kP_b\&2^{uv}R_v{}^{vw}U^kP_bS$	8●	0.8	0.8	0.8	0.8●	0	0	1	0.33●	0	0	0	0●	0	0	0	0◑	●●●●◑
10	Topology evolution of execution	$(^{uv}R_v{}^vRS\&2^{uv}R_v{}^vR^kP_bS)\text{-}^kP_b$	9●	1	0.67	1	0.89●	2	2	5	3◑	1	1	1	1◑	0	1	0	0.33●	●●●●
11		$(^{uv}R_v{}^vR^vR^{ws}U\&2^{uv}R_v{}^vR^vR^kP_b{}^{ws}U)\text{-}^kP_b$	12○	1	0.67	1	0.89●	5	5	8	6○	2	2	2	2○	0	1	0	0.33●	●●
12		$(^{uv}R_vS^wR\&2^{uv}R_v{}^vR^kP_bS)\text{-}^kP_b$	9●	0.67	0.67	0.67	0.67◑	2	2	4	2.67◑	1	1	1	1◑	0	1	0	0.33●	●●●◑
13		$(^{uv}R_vS\&^{uv}R_v{}^vR^kP_bS\&^{uv}R_v{}^{vw}U^kP_bS)\text{-}^kP_b$	8●	0.6	0.6	0.6	0.6◑	2	1	2	1.67●	0	0	0	0●	0	1	0	0.33●	●●●●◑
14		$(^{uv}R_v{}^vR^{vw}U\&^{uv}R_v{}^vR^kP_bS$ $\&^{uv}R_vS^kP_b{}^{ws}U)\text{-}^kP_b$	9●	0.27	0.53	0.27	0.36○	3	2	4	3◑	0	0	0	0●	0	1	0	0.33●	●●●◑
15		$(^{uv}R_v{}^vR^vR^wR\&^{uv}R_v{}^vR^vR^kP_b{}^{ws}U$ $\&^{uv}R_v{}^{vw}U^kP_bS)\text{-}^kP_b$	11◑	0.4	0.4	0.4	0.4○	4	4	5	4.33◑	0	0	0	0●	0	1	0	0.33●	●●●
16		$(^{uv}R_v{}^vR^wR\&2^{uv}R_vS^kP_b{}^{ws}U)\text{-}^kP_b$	9●	0.8	0.8	0.8	0.8●	0	0	1	0.33●	0	0	0	0●	0	1	0	0.33●	●●●●●
17		$(^{uv}R_v{}^{vw}U\&2^{uv}R_v{}^{vw}U^kP_bS)\text{-}^kP_b$	8●	0.8	0.8	0.8	0.8●	0	0	1	0.33●	0	0	0	0●	0	1	0	0.33●	●●●●●
18	Transmission	$^uR^uR^uR^vR^vR\&^{uv}R_v$	6○	0.5	-	0.5	0.5◑	5	-	5	5○	0	-	0	0●	1	-	1	1●	●●◑
19		$^uR^uR^{uv}U^uR\&^{uv}R_v$	5◑	0.33	-	0.33	0.33○	4	-	4	4◑	0	-	0	0●	1	-	1	1●	●●●
20		$^vR^{vu}U^uR^{uw}U\&^{uv}R_v$	5◑	0.57	-	0.57	0.57◑	3	-	3	3◑	0	-	0	0●	1	-	1	1●	●●●◑
21		$^vRSS\&^{uv}R_v$	4●	0.75	-	0.75	0.75●	0	-	0	0●	0	-	0	0●	1	-	1	1●	●●●●●

topologies, but a different adjusting topology with 2-DOF spherical motion generated by the universal joint in the primary limb. Hence, the spherical center and radius can be more easily determined to enhance the accessibility of adjusting in engineering. Furthermore, there are two metamorphic transmission mechanisms and one $^wP^vR^vR^vR$ primary transmission in each leg. Figure 12 simulates the implementation process of complete operation modes of ReLML. To explore the hostile extraterrestrial landform, adjusting mode matches the uneven terrain topography followed by landing. During the roving mode, the crawling gait is adopted with the locomotion sequence that: leg 2 swing, leg 1 swing, COG movement, leg 3 swing, leg 4 swing, to COG movement.

8 Conclusions

This paper presents the task-oriented topology system synthesis of ReLML for prototype construction. Main innovation points and contributions are:

(1) The legged mobile lander with three operation modes is first synthesized. Our group's preceding works just discuss the type synthesis with two modes, i.e., landing mode with 1R motion, and roving mode with 2R1T motion. This study redefines the landing mode with 2R1T motion (identical with Apollo and Chang'E landers), roving mode with 2R1T motion, and endows the ReLML with a totally novel adjusting mode with 3R motion. Thus, it will have better adaptability to hostile landform with better reasonable touchdown buffering motion.

(2) The reconfigurable mechanism theory is firstly brought into topology synthesis of legged mobile lander with three modes. The finite screw theory is applied to demonstrate metamorphic principles. Hence, theoretical connotation for the innovative design of multi-functional exploration probe is more credible. This work presents the procedure from unified mathematical representation, modes and source phase derivation, metamorphic joint and limb design, to the final structure assembly, etc.

(3) The topology system synthesis method of ReLML integrating active and passive metamorphoses is presented. The design of active metamorphic joint is carefully argued for good reliability, it can always ensure a brilliant flow of touchdown impact force through limb to main body after any adjusting pose, so the variable landing truss is always guaranteed with good buffering stably. Furthermore, the separation between transmission and execution facilitates to protect the fragile actuation unit like motor, sensor, encoder, reducer, etc.

(4) A 3D optimal selection matrix method is proposed to search for practicable topology, its dimensions contain three operation modes, five evaluation criteria (structural symmetry degree and geometric constraint complexity are first proposed), and two topology subsystems. Based on this, the 2D table presents the quantitative

correlations systematically. After combining the optimal execution and transmission respectively, the prototype topology is verified by simulating the whole task process.

Acknowledgements
Not applicable.

Authors' Contributions
YH conducted the theoretical study and modeling, completed the manuscript writing; ZL finished the simulation; GZ finished the polish and editing; WG gave overall guidance during modeling, analysis, and writing; JY and WL gave detailed guidance on the principle and design of prototype. All authors read and approved the final manuscript.

Authors' Information
Youcheng Han, born in 1993, is currently a PhD candidate at *State Key Lab of Mechanical System and Vibration, School of Mechanical Engineering, Shanghai Jiao Tong University, China*. His research interests include legged robot, landing gear, mechanism design.
Ziyue Li, born in 1996, is currently a PhD candidate at *State Key Lab of Mechanical System and Vibration, School of Mechanical Engineering, Shanghai Jiao Tong University, China*. His research interests include legged robot, motion planning, calibration.
Gaohan Zhu, born in 1998, is currently a PhD candidate at *State Key Lab of Mechanical System and Vibration, School of Mechanical Engineering, Shanghai Jiao Tong University, China*. His research interests include path planning, performance evaluation, 3D printing.
Weizhong Guo, born in 1970, is currently a professor and a PhD candidate supervisor at *State Key Lab of Mechanical System and Vibration, School of Mechanical Engineering, Shanghai Jiao Tong University, China*. His main research interests include modern mechanism, parallel robot, motion planning and design.
Jianzhong Yang, born in 1969, is currently a researcher at *Beijing Institute of Spacecraft System Engineering, China*. His main research interest is spacecraft mechanism.
Wei Liu, born in 1984, is currently a senior engineer at *Beijing Institute of Spacecraft System Engineering, China*. His main research interests include landing buffer mechanism, rover ramp mechanism, lock release mechanism.

Funding
Supported by National Natural Science Foundation of China (Grant No. 51735009), and State Key Lab of Mechanical System and Vibration Project of China (Grant No. MSVZD202008), and National Aerospace Science Foundation of China (040102).

Availability of data and materials
The datasets supporting the conclusions of this article are included within the article.

Declarations

Ethics approval and consent to participate
Not applicable.

Consent for publication
Not applicable.

Competing interests
The authors declare no competing financial interests.

Received: 8 June 2022 Revised: 8 May 2023 Accepted: 16 May 2023
Published online: 30 June 2023

References
[1] L Fang, F Gao. Type design and behavior control for six legged robots. *Chinese Journal of Mechanical Engineering*, 2018, 31(1).
[2] D Xi, F Gao. Type synthesis of walking robot legs. *Chinese Journal of Mechanical Engineering*, 2018, 31(1).
[3] NASA. Surveyor program results, NASA-SP-184. NASA, Washington D.C., USA, 1969.
[4] E M Galimov. Luna-Glob project in the context of the past and present lunar exploration in Russia. *J. Earth Syst. Sci.*, 2005, 114(6): 801-806.
[5] C Li, R Zhang, D Yu, et al. China's mars exploration mission and science investigation. *Space Sci. Rev.*, 2021, 217(4).
[6] M R Grover, B D Cichy, P N Desai. Overview of the Phoenix entry, descent, and landing system architecture. *J. Spacecraft Rockets*, 2011, 48(5): 706-712.
[7] D H Merchant, D T Sawdy. Monte Carlo dynamic analysis for lunar module landing loads. *J. Spacecraft Rockets*, 1971, 8(1): 48-55.
[8] C Li, W Zuo, W Wen, et al. Overview of the Chang'e-4 mission: opening the frontier of scientific exploration of the lunar far side. *Space Sci. Rev.*, 2021, 217(2).
[9] B H Wilcox, T Litwin, J Biesiadecki, et al. Athlete: A cargo handling and manipulation robot for the moon. *J. Field Robo*t, 2007, 24(5): 421-434.
[10] F Cordes, F Kirchner, A Babu. Design and field testing of a rover with an actively articulated suspension system in a Mars analog terrain. *J. Field Robot*, 2018, 35(7): 1149-1181.
[11] K Yin, Q Sun, F Gao, et al. Lunar surface soft-landing analysis of a novel six-legged mobile lander with repetitive landing capacity. *Proceedings of the Institution of Mechanical Engineers. Part C, Journal of Mechanical Engineering Science*, 2021: 2141051770.
[12] K Yin, S Zhou, Q Sun, et al. Lunar surface fault-tolerant soft-landing performance and experiment for a six-legged movable repetitive lander. *Sensors-Basel*, 2021, 21(17): 5680.
[13] N Rudin, H Kolvenbach, V Tsounis, et al. Cat-like jumping and landing of legged robots in low gravity using deep reinforcement learning. *IEEE T. Robot*, 2022, 38(1): 317-328.
[14] R Lin, W Guo, M Li, et al. Novel design of a legged mobile lander for extraterrestrial planet exploration. *Int. J. Adv. Robot. Syst.*, 2017, 14(6): 256006380.
[15] Y Han, C Zhou, W Guo. Singularity loci, bifurcated evolution routes, and configuration transitions of reconfigurable legged mobile lander from adjusting, landing, to roving. *ASME Journal of Mechanisms and Robotics*, 2021, 13(4): 1-11.
[16] R Lin, W Guo, M Li. Novel Design of legged mobile landers with decoupled landing and walking functions containing a rhombus joint. *Journal of Mechanisms and Robotics*, 2018, 10(6): 61017.
[17] Y Han, W Guo, F Gao, et al. A new dimension design method for the cantilever-type legged lander based on truss-mechanism transformation. *Mech. Mach. Theory*, 2019, 142(12): 103611.
[18] Y Han, W Guo, Z Peng, et al. Dimensional synthesis of the reconfigurable legged mobile lander with multi-mode and complex mechanism topology. *Mech. Mach. Theory*, 2021, 155(1): 104097.
[19] R Lin, W Guo, X Chen, et al. Type synthesis of legged mobile landers with one passive limb using the singularity property. *Robotica*, 2018, 36(12): 1836-1856.
[20] Y Han, W Guo. Novel design of the actuation-transmission system for legged mobile lander considering large impact. *The 15th IFToMM World Congress*, Kracow, Poland, 2019.
[21] Q Li, Z Huang, J M Hervé. Displacement manifold method for type synthesis of lower-mobility parallel mechanisms. *Science in China Series E-Engineering & Materials Science*, 2004, 47(6): 641-650.
[22] S Yang, T Sun, T Huang, et al. A finite screw approach to type synthesis of three-DOF translational parallel mechanisms. *Mech. Mach. Theory*, 2016, 104: 405-419.
[23] S Yang, T Sun, T Huang. Type synthesis of parallel mechanisms having 3T1R motion with variable rotational axis. *Mech. Mach. Theory*, 2017, 109: 220-230.
[24] T Sun, X Huo. Type synthesis of 1T2R parallel mechanisms with parasitic motions. *Mech. Mach. Theory*, 2018, 128: 412-428.
[25] T Sun, S Yang, T Huang, et al. A finite and instantaneous screw based approach for topology design and kinematic analysis of 5-axis parallel kinematic machines. *Chinese Journal of Mechanical Engineering*, 2018, 31(1).
[26] J S Dai, J R Jones. Matrix representation of topological changes in metamorphic mechanisms. *J. Mech. Design*, 2005, 127(4): 837-840.

[27] H Yan, C Kang. Configuration synthesis of mechanisms with variable topologies. *Mech. Mach. Theory*, 2009, 44(5): 896-911.
[28] S Li, J S Dai. Structure synthesis of single-driven metamorphic mechanisms based on the augmented Assur groups. *Journal of Mechanisms and Robotics*, 2012, 4(3).
[29] X Kong, C M Gosselin, P Richard. Type synthesis of parallel mechanisms with multiple operation modes. *J. Mech. Design*, 2007, 129(6): 595-601.
[30] B Chang, G Jin, J Dai. Type synthesis of metamorphic mechanism based on variable constraint screw theory. *Journal of Mechanical Engineering*, 2014, (5): 17-25. (in Chinese)
[31] Q Li, J M Herve. Parallel mechanisms with bifurcation of schoenflies motion. *IEEE T. Robot*, 2009, 25(1): 158-164.
[32] J Wei, J S Dai. Lie group based type synthesis using transformation configuration space for reconfigurable parallel mechanisms with bifurcation between spherical motion and planar motion. *J. Mech. Design*, 2019, 142(6): 1-41.
[33] J Wei, J S Dai. Reconfiguration-aimed and manifold-operation based type synthesis of metamorphic parallel mechanisms with motion between 1R2T and 2R1T. *Mech. Mach. Theory*, 2019, 139: 66-80.
[34] Y Liu, Y Li, Y Yao, et al. Type synthesis of multi-mode mobile parallel mechanisms based on refined virtual chain approach. *Mech. Mach. Theory*, 2020, 152(10): 103908.
[35] Y Tian, D Zhang, Y Yao, et al. A reconfigurable multi-mode mobile parallel robot. *Mech. Mach. Theory*, 2017, 111: 39-65.
[36] J Wu, Y Yao. Design and analysis of a novel walking vehicle based on leg mechanism with variable topologies. *Mech. Mach. Theory*, 2018, 128: 663-681.
[37] X Pei, J Yu. A visual graphic approach for mobility analysis of parallel mechanisms. *Frontiers of Mechanical Engineering*, 2011, 6(1): 92-95.
[38] W Ma, J Yu, Y Yang. Graphical design methodology of multi-degrees-of-freedom tuned mass damper for suppressing multiple modes. *Journal of Vibration and Acoustics*, 2021, 143(1).
[39] H Shen, T Yang, J Li, et al. Evaluation of topological properties of parallel manipulators based on the topological characteristic indexes. *Robotica*, 2019: 1-19.
[40] H Shen, Y Tang, G Wu, et al. Design and analysis of a class of two-limb non-parasitic 2T1R parallel mechanism with decoupled motion and symbolic forward position solution - influence of optimal arrangement of limbs onto the kinematics, dynamics and stiffness. *Mech. Mach. Theory*, 2022, 172: 104815.
[41] H Liu, K Xu, H Shen, et al. Type synthesis of 1T2R parallel mechanisms using structure coupling-reducing method. *Chinese Journal of Mechanical Engineering*, 2019, 32(1).
[42] J He, F Gao, X Meng, et al. Type synthesis for 4-DOF parallel press mechanism using GF set theory. *Chinese Journal of Mechanical Engineering*, 2015, 28(4): 851-859.
[43] M Barej, T Mannheim, S Kurtenbach, et al. Application-oriented mechanism design at the example of a packaging machine. *The 14th World Congress in Mechanism and Machine Science*, Taiwan, China, 2015: 681-686.
[44] G Gogu. Structural synthesis of parallel robots. part 1: Methodology. *Springer*, Dordrecht, Netherlands, 2008.